IEEE Access
Multidisciplinary | Rapid Review | Open Access Journal

Received 14 March 2024, accepted 5 April 2024, date of publication 16 April 2024, date of current version 24 April 2024.

Digital Object Identifier 10.1109/ACCESS.2024.3389824

RESEARCH ARTICLE

PMBM Filtering With Fusion of Target-Provided and Exteroceptive Measurements: Applications to Maritime Point and Extended Object Tracking

AUDUN G. HEM, MARTIN BAERVELDT, AND EDMUND F. BREKKE, (Senior Member, IEEE)
Department of Engineering Cybernetics, Norwegian University of Science and Technology, 7034 Trondheim, Norway

Corresponding author: Audun G. Hem (audun.g.hem@ntnu.no)

This work was supported in part by the Research Council of Norway under Project 309230 SFI Autoship and Project 295033 Autosit, in part by DNV, in part by Kongsberg, in part by Maritime Robotics. The research leading to these results has also received funding from the European Union's Horizon 2020 research and innovation programme under the Marie Skłodowska-Curie grant agreement No 955.768 (MSCA-ETN AUTOBarge). This publication reflects only the authors' view, exempting the European Union from any liability. Project website: http://etn-autobarge.eu/.

ABSTRACT In recent years, the Poisson multi-Bernoulli mixture (PMBM) filter has been established among the state-of-the art methods in target tracking. We present a method for including target-provided measurements in said filter, both when using it to track extended objects and point targets. We use messages from the Automatic identification system as an example of target-provided measurements, and radar and LiDAR as examples of exteroceptive sensors. In the point target case, we utilize several different kinematic models in parallel through the interacting multiple models framework, and compare the presented method to several common trackers and other PMBM filter configurations. The results show that our method outperforms similar methods when target-provided measurements are available. The point target variant is also shown to work in a closed-loop collision avoidance experiment in a maritime environment, demonstrating its feasibility for use in real-world applications. For the extended object tracking case, we expand upon the Gaussian process PMBM filter. The extended object method is evaluated on both simulated and experimental data, and is shown to improve the tracking performance when including target-provided measurements in comparison to when it only uses exteroceptive measurements.

INDEX TERMS Multi-target tracking, data fusion, AIS, radar, LiDAR, PMBM, extended object tracking, maritime target tracking.

I. INTRODUCTION

To bridge the gap between the physical and the digital world, one of the key problems is how to make any digital system understand what is happening around it. An approach to enable this understanding is to use sensors to measure the physical world, and then process the data received from the sensors. This is what is done in target tracking, where measurements collected from the surrounding area are used to estimate the properties of the targets inhabiting it.

Target tracking is, however, not a trivial problem. When faced with a set of noisy measurements, it is not always clear which measurements belong to which target, and how to combine the measurements to form a coherent picture. The problem is further complicated by the fact that the number of targets is unknown and may change over time. Hypothesized targets must be initialized, and the measurements have to be associated to the target they originated from. Only when the measurements have been associated to a target can a filtering method be used to estimate the target state. The joint estimation of the number of targets and their states is denoted as multi-target tracking [1]. The problem of finding the correct association is further complicated by the presence of false alarms and missed detections. Several measurements can also originate from the same target, which requires either clustering of the measurements, or a method which allows for

The associate editor coordinating the review of this manuscript and approving it for publication was Tao Wang.

multiple measurements to be associated to the same target. The two approaches are called point target tracking and extended object tracking, respectively.

In the last decades, many new multi-target tracking methods have been developed. The one used in this paper is the Poisson multi-Bernoulli mixture (PMBM) filter [2]. The PMBM filter is based on Random Finite Sets (RFS), specifically a potentially detected target is modelled as a Bernoulli RFS and the set of undetected targets is modelled as a Poisson point process (PPP). The PMBM filter has been shown to be among the state-of-the-art methods in target tracking [2], [3], [4], and has also been used for extended object tracking [5], [6], [7]. Furthermore, the interacting multiple model (IMM) filter [8] can be used to provide more flexibility in the modeling of the target behavior. The IMM filter uses a set of motion models, and switches between these depending on the current behavior of the target. The method has been used together with many tracking methods, including the PMBM filter [9].

Target tracking is used for a multitude of applications, but we focus on that of maritime situational awareness. For safe and efficient navigation at sea, it is important to correctly understand the surrounding area and the other vessels inhabiting it. Many ships employ, for example, maritime radars for this purpose, which can supplement the captain's situational awareness. Improved situational awareness was also the reason for introducing the Automatic identification system (AIS) [10], with which ships can relay information to surrounding vessels. The information can include their position, course, speed, identity, ship dimensions, and much more. For the human eye it is relatively intuitive to understand the information from these sensors when plotted on a map, and together with what is seen on the sea combine it to form a coherent picture of the surrounding area. This approach is, however, prone to human error, and ignores potentially valuable information that is not directly observable.

To further improve situational awareness at sea, one can use target tracking. This allows for the estimation of target speed, course, position, and the uncertainty of said quantities. The tracker may discover something the captain has missed, thus removing some of the potential for human error. Numerical estimates for the surrounding targets are also essential if these are to be used in decision making processes by anything other than a human. An example of this is the use of target tracking in collision avoidance systems, where the tracker may be used to predict the future position of the targets, and thus determine if a collision is likely to occur [11].

Most target tracking research has focused on how to track targets by use of exteroceptive sensors, such as radar and LiDAR. Recently, however, several methods have been developed to include target-provided information in target trackers [12], [13], [14], [15]. The methods differ from each other in important ways but share similarities in their general approach to the received information, namely that it is somewhat unreliable but nevertheless provide very valuable information when used correctly.

This paper combines many of the recent innovations regarding the PMBM filter and the use of target-provided information in target tracking. We present a method for including such information in the IMM-PMBM filter, using the model assumptions from [15]. Furthermore, we show how to use target-provided information together with an extended object tracking method, a PMBM with a Gaussian process extent model (GP-PMBM) [6]. The extended object tracker and the point measurement tracker are evaluated using both simulated and experimental data. Additionally, the point measurement tracker is used in a closed-loop collision avoidance experiment that demonstrates its feasibility for use in real-world applications.

The paper is organized as follows. Section II provides a brief explanation of relevant target tracking methods and concepts, together with an overview of previous work on use of target-provided data. In Section III we present the general model used to describe the targets and measurements. A general PMBM filter for use with target-provided measurements is described in Section IV, and it is specified for the point target and the extended object cases in Section V. The test setups and results for the point target case are presented in Section VI, and for the extended object case in Section VII. Lastly, we conclude the paper in Section VIII.

II. BACKGROUND

The detections, or measurements, provided by the sensors will have some degree of inaccuracy relative to the true target positions. The inaccuracies, or measurement noise as it is often denoted, can be mitigated by use of filtering. Examples of widely used filtering methods in target tracking are Kalman filters and particle filters, of which the Kalman filter is a linear method, and the particle filter is a sampling-based non-linear method. This solves the problem of noisy measurements, but not the problem of false alarms, missed detections, and the ambiguity of which measurements belong to which target.

A. SINGLE-SCAN TARGET TRACKING

The probabilistic data association (PDA) filter [16] is one of the early methods designed to solve the data association problem, as the problem of deciding which measurements come from the target is usually denoted. It calculates the probability of association between the measurements and the target by considering the predicted position of the target and comparing this to the received measurements while taking the uncertainty of the prediction and the measurements into account. In this way, it is able to account for the possibility of false alarms and missed detections.

Further development resulted in the joint PDA (JPDA) filter [17], which extended the PDA filter to also account for the existence of multiple targets, and thus the possibility of measurements originating from different targets. Whereas the PDA filter assumes that only a single target is present, the JPDA filter assumes that some known number of targets are present. The actual number of targets is, however, usually not actually known, and several methods have been developed

to initialize tracks based on the received measurements [18]. One of the solutions is found in the integrated PDA (IPDA) filter [19], and its multi-target version the joint integrated PDA (JIPDA) filter [20]. Here, target existence is not assumed, and the existence probability is calculated for each track that estimates a hypothesized target. Furthermore, the methods have been extended to work with the IMM filter, which uses several kinematic models for predicting the target state and switches between them depending on the estimated behavior of the target [8], [21].

Each time step, the PDA filter and its derived methods compute updated estimates based on the estimates from the previous time step and the measurements from the current time step. If several measurements have been received, their impact on the updated estimate depends on the association probability between the measurement and the estimate. If the estimates are represented as Gaussian distributions, this means that the updated estimate will be a Gaussian mixture with the components representing the estimate conditioned on different measurements, that is usually reduced to a single Gaussian before the next time step. This approximation ensures that the target trackers are computationally tractable, but it also means that temporal information is lost.

B. MULTI-SCAN TARGET TRACKING

Multi hypothesis tracking (MHT) [22] is a different approach to the data association problem. Here, the data association is solved by considering all possible associations between the measurements and the estimates. For each association, the estimate is updated based on the measurement, and the different combinations are used as the basis for new associations the next time new measurements arrive. This process results in a tree structure starting with the first detection and branches to the possible successive detections. A track hypothesis in the tree is a path from the root to one of the leaves, where said leaf is the estimated target state at the current time. This way of solving the multi-target tracking problem is denoted as multi-scan tracking, as opposed to the single-scan methods described above. However, the tree structure grows exponentially and quickly becomes intractable to maintain. To mitigate this, branches are pruned to remove the most unlikely hypotheses.

The PMBM filter is also a multi-scan multi-target tracking method. As opposed to what is the case for MHT, it allows for more mathematically rigorous procedures for initialization and termination of tracks. Each time new measurements are received, all possible associations between the new measurements and the Bernoulli components of the multi-Bernoulli mixture from the previous time step give rise to new Bernoulli components. Bernoulli distributions representing potential new targets are created based on incoming measurements with basis in a PPP. As for the MHT algorithm, this results in an exponentially growing number of Bernoulli components, and this is mitigated by a combination of pruning and only keeping a fixed number of possible global hypotheses. A global hypothesis is a set of Bernoulli components which together form a complete set of possible associations between the measurements and the targets. The PMBM filter has been further developed to work with the IMM filter [9].

C. EXTENDED OBJECT TRACKING

Most early works on multi-target tracking assumes that objects only generate a single measurement, the so-called point target assumption. Relaxing this assumption to allow targets to generate a varying number of measurements leads to the problem of extended object tracking [23]. The manner in which an extended object generates measurements is most commonly modelled as an inhomogeneous PPP. The Poisson rate governs the expected number of measurements, and a specific spatial distribution indicates how these measurements are spatially distributed across the target [24]. This spatial distribution allows us to estimate the shape and size of an object, which is referred to as object extent. Initial approaches used elliptical shapes as priors for the spatial distribution, this is commonly referred to as the random matrix model [25]. The extent of the object is then modelled by a symmetric and positive definite $d \times d$ matrix called the shape matrix, where d is the dimension of the object. The elements of this matrix are then estimated according to the spatial distribution of the measurements. This model is very popular because it is a linear model. Another approach instead models the extent as a generic star-convex shape by parametrizing the shape contour. This enables the modelling of more complex shapes, but it should be noted that the estimation problem then becomes non-linear [26]. This method is well suited to modeling contour generated measurements, such as those generated by LiDARs. The shape contour is parametrized by a radius function which can be estimated by a variety of techniques, the seminal paper used Fourier series, but today the most common method is to use Gaussian processes [27]. The Gaussian process method also allows the use of specific symmetry properties of the tracked objects when estimating their extent.

D. MULTIPLE EXTENDED OBJECT TRACKING

When tracking multiple extended objects, the data association becomes harder because each target can generate an unknown number of measurements. The first theoretical framework for a multiple extended object tracker was derived from the probability hypothesis density (PHD) filter by using the above-mentioned PPP model [28]. This filter was then implemented using the random matrix model, and an inverse Wishart distribution was used for estimation of the shape matrix [29]. This approach was augmented by estimating the Poisson rate governing the expected number of generated measurements for each target using a gamma distribution [30]. Combining them resulted in the gamma Gaussian inverse Wishart (GGIW) model [31]. Later developments explored extended object formulations of other types of filters, such as the PMBM filter [5]. Initially it was presented with the GGIW model, but the same formulation has been

used to implement a PMBM filter using the Gaussian process model augmented with a gamma distribution [6]. This filter has also been demonstrated on maritime LiDAR data.

E. FUSION OF EXTEROCEPTIVE SENSOR MEASUREMENTS AND TARGET-PROVIDED INFORMATION

Exteroceptive and target-provided measurements are very different in nature. This is the case both for the information they provide, and how the information is received. The exteroceptive measurements usually arrive periodically, and the quality of the measurements depends on the position of the target relative to the sensor. Furthermore, the information contained in the measurements is often limited to the position and possibly the speed of the reflecting surface. The target-provided measurements, however, have less limitations in what information they provide. The information is collected by the target itself, and the precision of the data is as such not dependent on where the target is located. However, by not controlling the data collection process, the quality of the received data is not guaranteed and often difficult to assess. Furthermore, whereas the exteroceptive measurements are usually received periodically, the target-provided measurements are received sporadically with practically unknown intervals. This demands care when using the information, and when designing models for including it in the target tracking process.

In recent years, several methods for measurement level fusion of target-provided information and exteroceptive measurements have been proposed. Measurement level fusion entails updating the estimates based on measurement data from different sensors, as opposed to the approach taken in track level fusion, where the estimates are only updated based on a single sensor and then fused with estimates based on input from other sensors. In [12], the authors propose a measurement level fusion method for combining AIS and radar measurements in context of the JPDA filter. The authors take the transmitted ID information into account and present a method for applying the IDs to targets using Bayesian inference. Furthermore, they consider the physical nature of AIS messages, with their infrequent transmission and absence of false alarms. The results show the benefit of utilizing AIS messages, and the increased performance of the measurement level fusion approach relative to track level fusion approaches.

A somewhat different approach is found in [13], where a solution is presented for a tracker that utilizes belief propagation and a particle filter. The problem is formulated as a factor graph, with calculations consisting of passing messages between nodes in the graph. The work also considers initialization of tracks using both exteroceptive and target-provided measurements, and the time discrepancy between the different measurement types. In [15] a method which utilizes AIS messages in a JIPDA filter is presented. It incorporates initialization of tracks based on all measurement types, and accounts for timing differences between them. The method uses an IMM filter, and also allows a target to enter an invisible state, mimicking the effects encountered when a target is occluded. Both aforementioned methods estimate the ID information probabilistically, and thus allow for the handling of incorrect ID information.

Lastly, both the MHT algorithm and the PMBM filter have previously been used together with target-provided information. An AIS-guided MHT is described in [32]. Here, the AIS information is modeled as if it was provided by another exteroceptive sensor, with artificial models for false alarms and missed detections. Furthermore, the transmitted IDs are assumed to always be correct, and any errors are instead removed in the pre-processing stage. The method is shown to improve the tracking performance relative to a MHT without AIS information. In [14] the authors present a method for using AIS information in the PMBM filter. They take a similar approach as for the MHT variant and model the AIS information similarly to exteroceptive measurements. Furthermore, the transmitted IDs are not explicitly considered in the calculations but are used to label the tracks corresponding to AIS-transmitting targets.

F. RELATION TO PREVIOUS WORK

Much of the mathematical framework used in this paper is based on the work in [15]. This is possible because the tracker in [15], even though it ultimately is a JIPDA-type tracker, can be seen as a special case of the PMBM filter. It is an extension of the IMM-JIPDA tracker with visibility modeling presented in [33], where the steps needed to go from the PMBM filter to a JIPDA-type filter are thoroughly presented. The link between the two filters can be explained by using the track-oriented marginal multiple target multi-Bernoulli/Poisson (TOMB/P) filter as an intermediate step. Williams notes in [2, Sec. IV-A] that the TOMB/P filter results from forcing the individual track hypotheses in a global PMBM hypothesis to be independent. This approximation results in tracks formed by the marginal track-to-measurement association probabilities, as is done in the JPDA and JIPDA filters. By assuming that new targets are born according to a stationary birth density, and by neglecting the influence of unknown targets when calculating the association probabilities, the TOMB/P filter becomes identical to a JIPDA filter. Despite these differences, the formulations in [15] and [33] are similar enough to make the transition from an IMM-JIPDA filter which utilizes target-provided information to an IMM-PMBM filter relatively straightforward. Note that a visibility state is present in both [15] and [33], which models the possibility of a target being occluded. This state is omitted in this paper but is possible to include without much effort.

III. MODEL

The model used to describe the targets and measurements is similar to the one presented in [15], which itself is based in the model underlying the PMBM filter. The model describes how the targets are represented, how they are created, and how they evolve over time. Furthermore, it describes how

the measurements and the information they contain relate to the targets. Thus, the model forms the framework we use to later describe how to estimate the target states based on the measurements.

A. THE POISSON MULTI-BERNOULLI MIXTURE

In general, the PMBM filter models the targets as the union of undetected targets and detected targets. The undetected targets are represented as a PPP, whereas the hypothesized detected targets are modeled as a multi-Bernoulli mixture (MBM). The combination of a PPP and an MBM ensures a conjugate prior in the context of recursive Bayesian estimation. We write the multi-target density as

$$f(X) = \sum_{Y \uplus W = X} f^{ppp}(Y) f^{mbm}(W) \tag{1}$$

where X is the set of all targets, Y is the set of undetected targets, W is the set of detected targets, $\uplus$ denotes the disjoint union, $f^{ppp}(\cdot)$ is the PPP, and $f^{mbm}(\cdot)$ is the MBM. The PPP is defined as

$$f^{ppp}(X) = \exp(-\int \mu(\tilde{\mathbf{x}}) \mathrm{d}\tilde{\mathbf{x}}) \prod_{\mathbf{x} \in X} \mu(\mathbf{x}) \tag{2}$$

where $\mu(\tilde{\mathbf{x}})$ is the intensity function and the notation $\tilde{\cdot}$ indicates marginalization over a variable. Boldface notation is used for vectors. Furthermore, the MBM is defined as

$$f^{mbm}(X) \propto \sum_{j} \sum_{X_1 \uplus \ldots \uplus X_n = X} \prod_{i=1}^{n} w^{j,i} f^{j,i}(X_i). \tag{3}$$

The first sum accounts for all global hypotheses, and the second for all hypothesized targets within the global hypothesis. $w^{j,i}$ is the weight and distribution of potentially detected target i in global hypothesis j. The distribution $f^{j,i}(X_i)$, a Bernoulli RFS, is defined as

$$f^{j,i}(X^i) = \begin{cases} 1 - r^{j,i} & \text{if } X^i = \emptyset \\ r^{j,i} p^{j,i}(\mathbf{x}) & \text{if } X^i = \{\mathbf{x}\} \\ 0 & \text{otherwise} \end{cases} \tag{4}$$

where $r^{j,i}$ is the existence probability, and $p^{j,i}(\mathbf{x})$ is the state density.

B. THE HYBRID STATE SPACE

The full state $\mathbf{y}$ of a target can contain both discrete and continuous states. Such a combination is often denoted as a hybrid state [34, p. 411]. The continuous part of the state is denoted as $\mathbf{x}$, and typically contains information such as position, velocity, or target extent. The discrete states can contain information such as target ID, what kinematic model the target is following, or if the target is occluded. In this section and the next, the exact information contained in the states is not important, but rather how they relate to each other, and how they evolve.

Nevertheless, we select two discrete states to illustrate the concepts, which are also useful later, namely the ID τ and the kinematic model s. The distribution of the hybrid state can be written as

$$p(\mathbf{x}, \tau, s) = p(\mathbf{x}|\tau, s) p(s|\tau) p(\tau). \tag{5}$$

Furthermore, the actual ID of a target is assumed to not change over time, whereas the kinematic model a target moves according to can change. For any discrete state with the same properties as either the ID or the kinematic model, the following can also be used to describe how to incorporate that state into the model.

C. NEW TARGETS

We assume that new targets are born according to a PPP with intensity $b(\mathbf{y})$. A birth intensity with N_b components is defined as

$$b(\mathbf{y}) = \sum_{i=1}^{N_b} w^{b,i} p^{b,i}(\tau) p^{b,i}(s|\tau) p^{b,i}(\mathbf{x}|s, \tau). \tag{6}$$

Here, $p^{b,i}(\tau)$ is the distribution of the IDs τ, $p^{b,i}(s|\tau)$ is the distribution of the kinematic models s, and $p^{b,i}(\mathbf{x}|s, \tau)$ is the distribution of the state $\mathbf{x}$. As the hybrid state includes both discrete and continuous states, the PPP is what is denoted as a marked PPP, equivalent to a PPP on the Cartesian product of the continuous space of the kinematic density and the discrete spaces of the other states. Under the assumption that the distributions of all states are independent of other elements in the marked PPP, it nevertheless inherits the properties of a PPP, and can be used interchangeably in the PMBM. This means that a restriction of unique IDs across targets can not be enforced, as it would break the independence assumption underlying the PPP.

We assume that the IDs of unknown targets are independent and identically distributed (i.i.d.) with an initial prior distribution

$$p^{b,i}(\tau) = \begin{cases} \xi^{b,0} & \text{if } \tau = 0 \\ \dfrac{1 - \xi^{b,0}}{|\mathcal{V}| - 1} & \text{if } \tau > 0. \end{cases} \tag{7}$$

Here, $\xi^{b,0}$ denotes the initial probability of a specific ID, whereas $|\mathcal{V}|$ is the number of possible IDs and $\tau \in \mathcal{V}$. The first case accounts for the probability of a target not having an ID, whereas the second case accounts for the probability of a target having an ID. For the latter case, the probability is uniformly distributed among all possible IDs. Furthermore, the kinematic models s are assumed to be i.i.d. with an initial distribution μ_s^0.

D. TARGET EVOLUTION

For the different variables, we use the subscript k to indicate that we are considering their value at the current time step, and with $k-1$ we indicate the previous time step.

Each target is assumed to survive a duration of T with probability

$$P_S(T) = P_{S_c}^T \tag{8}$$

where S_c is the survival probability per time unit, usually seconds.

The target IDs do not change over time, whereas the kinematic model can change between time steps as part of a Markov chain. The transition matrix π contains the Markov chain probabilities of a change occurring, whereas the target ID transition is modeled as a Kronecker delta δ. The kinematic transition density depends on the kinematic model, and we can write the prediction of a target as

$$f_{\mathbf{y}}(\mathbf{y}_k|\mathbf{y}_{k-1}) = f_{\mathbf{x}}(\mathbf{x}_k|\mathbf{x}_{k-1}, \tau_k, s_k)\pi^{s_{k-1}s_k}\delta^{\tau_{k-1}\tau_k}. \quad (9)$$

This transition is that of a target with ID τ_{k-1} and kinematic model s_{k-1} at the previous time step, and target ID τ_k and kinematic model s_k at the current time step.

E. MEASUREMENTS

The detection probability of a target by way of exteroceptive sensors is assumed constant in both time and space and is denoted as $P_D(\mathbf{y}) = P_D$. For the target-provided measurements, the detection probability is designed to more precisely reflect their physical reality. This is done by setting the detection probability to 1 if a target-provided measurement is received, and 0 otherwise. We express this as

$$P_D(\mathbf{y}) = \begin{cases} 1 & \text{if a measurement is received} \\ 0 & \text{otherwise.} \end{cases} \quad (10)$$

Only the exteroceptive sensors are assumed to provide false alarms, referred to as clutter, and the clutter is modeled as a PPP with intensity $\lambda(Z)$. The intensity can depend on measurement position but is assumed to not change over time. For the target-provided measurements, the absence of clutter is modeled by using a PPP with intensity 0.

We assume that the exteroceptive measurements are synchronized, and all detections in each individual scan come from time step k. This is, for most sensors, an approximation. If needed, the time disparity between detections in a scan can be accounted for by relatively simple means [35]. The likelihood for a set of exteroceptive measurements is $f^{ex}_{\mathbf{z}}(Z_k|\mathbf{y}_k)$, where Z_k is a set of measurements. For point target tracking, the set is either empty, or contains a single measurement. For extended object tracking, the set can contain several measurements. The information provided by the exteroceptive measurements is assumed to only contain the position of the detections, or potentially also the speed of the reflecting surface.

The target-provided measurements are not assumed to be synchronized. They can arrive at any time, and furthermore, they arrive at different times for different targets. The likelihood is denoted as $f^{tp}_{\mathbf{z}}(Z_k|\mathbf{y}_k)$. We assume that a set of target-provided measurements will contain at most a single measurement. As opposed to the case for the exteroceptive measurements $\mathbf{z}_k$ can now also contain additional information, such as ID and target dimensions. We assume that, when conditioned on the target state, the information in the measurements is independent of other information contained in the measurement. Furthermore, we keep in mind that the detection probability is 1 if a measurement is received. This means that the likelihood of a set with a measurement containing, for example, kinematic information $\mathbf{p}$, ID τ, length z^L, and width z^W can be decomposed as

$$f^{tp}_{\mathbf{z}}(Z_k|\mathbf{y}_k) = f^{tp}_{\mathbf{p}}(\mathbf{p}_k|\mathbf{y}_k)f^{tp}_{\tau}(\tau_k|\mathbf{y}_k)f^{tp}_{L}(z^L|\mathbf{y}_k)f^{tp}_{W}(z^W|\mathbf{y}_k) \quad (11)$$

whereas a set without a measurement has a likelihood of 1 because the detection probability is 0 when no measurement is received.

IV. METHOD

From the previous time step $k-1$, we assume that the Poisson component representing an unknown target is given by

$$u_{k-1}(\mathbf{y}_{k-1}) = \sum_{i=1}^{N} w^{u,i}_{k-1} p^{u,i}_{k-1}(\tau_{k-1}) p^{u,i}_{k-1}(s_{k-1}) p^{u,i}_{k-1}(\mathbf{x}_{k-1}|s_{k-1}, \tau_{k-1}) \quad (12)$$

which is a sum of mixture components where $w^{u,i}_{k-1}$ is the weight of component i. A potentially detected target i in a global hypothesis j at the previous time step is represented by a Bernoulli distribution with existence probability $r^{j,i}_{k-1}$, weight $w^{j,i}_{k-1}$ and state density

$$p^{j,i}_{k-1}(\mathbf{y}_{k-1}) = p^{j,i}_{k-1}(\mathbf{x}_{k-1}|\tau_{k-1}, s_{k-1}) \times p^{j,i}_{k-1}(s_{k-1}|\tau_{k-1}) p^{j,i}_{k-1}(\tau_{k-1}). \quad (13)$$

For ease of notation, we henceforth write $p^{\cdot,i}_{k-1}(\tau_{k-1})$ as $\xi^{\cdot,i\tau}_{k-1}$ and $p^{\cdot,i}_{k-1}(s_{k-1}|\tau_{k-1})$ as $\mu^{\cdot,i\,s\tau}_{k-1}$.

A. PREDICTION

We find the expressions for the prediction by use of the expressions from [15, Sec. V] and [36, Sec. V]. For the Poisson component, we get that the predicted intensity is

$$u_{k|k-1}(\mathbf{y}_k) = b_k(\mathbf{y}_k) + P_S(T) \sum_{i=1}^{N} w^{u,i} \mu^{u,i\,s\tau}_{k|k-1} \xi^{u,i\tau}_{k|k-1} p^{u,i}_{k|k-1}(\mathbf{x}_k|s_k, \tau_k) \quad (14)$$

whereas the predicted Bernoulli components are

$$p^{j,i}_{k|k-1}(\mathbf{y}_k) = \mu^{j,i\,s\tau}_{k|k-1} \xi^{j,i\tau}_{k|k-1} p^{j,i}_{k|k-1}(\mathbf{x}_k|s_k, \tau_k). \quad (15)$$

Furthermore, we predict the existence probability and discrete states in the hybrid state as

$$r^{\cdot,i}_{k|k-1} = r^{\cdot,i}_{k-1} P_S(T) \quad (16)$$

$$\xi^{\cdot,i\tau}_{k|k-1} = \xi^{\cdot,i\tau}_{k-1} \quad (17)$$

$$\mu^{\cdot,i\,s\tau}_{k|k-1} = \sum_{\tilde{s}} \mu^{\cdot,i\tilde{s}\tau}_{k-1} \pi^{\tilde{s}s}(T). \quad (18)$$

where $\cdot$ denotes that the expressions are valid for both unknown and potentially detected targets. The kinematic density is predicted as

$$p^{\cdot,i}_{k|k-1}(\mathbf{x}_k|\tau_k, s_k) = \int f_{\mathbf{x}}(\mathbf{x}_k|\tau_k, s_k, \tilde{\mathbf{x}}) p^{\cdot,i}_{k-1}(\tilde{\mathbf{x}}|\tau_k, s_k) \mathrm{d}\tilde{\mathbf{x}} \tag{19}$$

where

$$p^{\cdot,i}_{k-1}(\tilde{\mathbf{x}}|\tau_k, s_k) = \sum_{\tilde{s}} \frac{\mu^{\cdot,i\tau\tilde{s}}_{k-1} \pi^{\tilde{s}s}(T) p^{\cdot,i}_{k-1}(\tilde{\mathbf{x}}|\tau_k, s_k, \tilde{s})}{\sum_{\tilde{s}} \mu^{\cdot,i\tau\tilde{s}}_{k-1} \pi^{\tilde{s}s}(T)}. \tag{20}$$

B. UPDATE

The posterior is also found by use of [15, Sec. V] in combination with [36, Sec. V]. Three different types of updates must be considered:

- Update of undetected targets.
- Update of new potentially detected targets.
- Update of previously potentially detected targets.

The update of undetected targets only involves updating the weight. For convenience, the unknown target intensity is rewritten as

$$u_k(\mathbf{y}_k) = \sum_{i=1}^{N_u} w^{u,i}_{k|k-1} p^{u,i}_{k|k-1}(\mathbf{y}_k). \tag{21}$$

We update the weights by multiplying them with the probability of a missed detection

$$w^{u,i}_k = w^{u,i}_{k|k-1}(1 - P_D). \tag{22}$$

1) UPDATE OF NEW POTENTIALLY DETECTED TARGETS

When a potential new target is detected, a new Bernoulli component is initialized. We need to find the Bernoulli component's existence probability $r^{j,i}_k(Z_k)$, state density $p^{j,i}_k(\mathbf{y}_k|Z_k)$, and weight $w^{j,i}(Z_k)$. This is done by updating the unknown target intensity with some non-empty subset Z_k of all the received detections. We have from [36, Sec. V] that

$$r^{j,i}_k(Z_k) = \frac{e(Z_k)}{\rho(Z_k)} \tag{23}$$

$$p^{j,i}_k(\mathbf{y}_k|Z_k) = \sum_{i=1}^{N_u} w^i(Z_k) p^{u,i}_k(\mathbf{y}_k|Z_k) \tag{24}$$

where

$$\begin{aligned} e(Z_k) &= \sum_{i=1}^{N_u} w^{u,i} f^{u,i}_{\mathbf{z}}(Z_k|\mathbf{y}_k) \\ \rho(Z_k) &= e(Z_k) + \lambda(Z_k) \\ w^i(Z_k) &\propto w^{u,i}_{k|k-1} f^{u,i}_{\mathbf{x}}(Z_k|\mathbf{y}_k). \end{aligned} \tag{25}$$

The weight $w^{j,i}_k$ of the new Bernoulli component in a global hypothesis j has value $\rho(Z_k)$ if the global hypothesis includes the new target, and otherwise the weight is set to 1 with the existence probability set to 0. Furthermore, we need to find expressions for $p^{u,i}_k(\mathbf{y}_k|Z_k)$ and $f^{u,i}_{\mathbf{x}}(Z_k|\mathbf{y}_k)$. We provide these on a general form that holds for exteroceptive measurements and target-provided information in both point target and extended object tracking, and from [15, Sec. V] we get that

$$p^{\cdot,i}_k(\mathbf{y}_k|Z_k) = p^{\cdot,i}_{k|k-1}(\mathbf{x}_k|\tau_k, s_k, Z_k) \mu^{\cdot,is\tau}_k \xi^{\cdot,i\tau}_k \tag{26}$$

where

$$\begin{aligned} &p^{\cdot,i}_k(\mathbf{x}_k|\tau_k, s_k, Z_k) \\ &= \frac{f^{\cdot,i}_{\mathbf{z}}(Z_k|\tau_k, s_k, \mathbf{x}_k) p^{\cdot,i}_{k|k-1}(\mathbf{x}_k|\tau_k, s_k)}{l^{\cdot,i\tau s}} \end{aligned} \tag{27}$$

and

$$\mu^{\cdot,is\tau}_k = \frac{\mu^{\cdot,i\tau s}_{k|k-1} l^{\cdot,i\tau s}}{\sum_{\tilde{s}} \mu^{\cdot,i\tau\tilde{s}}_{k|k-1} l^{\cdot,i\tau\tilde{s}}} \tag{28}$$

$$\xi^{\cdot,i\tau}_k = \frac{\xi^{\cdot,i\tau}_{k|k-1} \sum_{\tilde{s}} \mu^{\cdot,i\tau\tilde{s}}_{k|k-1} l^{\cdot,i\tau\tilde{s}}}{\sum_{\tilde{\tau}} \xi^{\cdot,i\tilde{\tau}}_{k|k-1} \sum_{\tilde{s}} \mu^{\cdot,i\tilde{\tau}\tilde{s}}_{k|k-1} l^{\cdot,i\tilde{\tau}\tilde{s}}}. \tag{29}$$

Furthermore, we have that

$$l^{\cdot,i\tau s} = \int f^{\cdot,i}_{\mathbf{z}}(Z_k|\tau_k, s_k, \tilde{\mathbf{x}}) p^{\cdot,i}_{k|k-1}(\tilde{\mathbf{x}}|\tau_k, s_k) \mathrm{d}\tilde{\mathbf{x}}. \tag{30}$$

2) UPDATE OF PREVIOUSLY POTENTIALLY DETECTED TARGETS

A potentially detected target can either be updated based on a detection or a missed detection. First, we define the combined likelihood of a measurement set across all discrete states as

$$L^{j,i} = \sum_{\tilde{\tau}} \xi^{j,i\tilde{\tau}}_{k|k-1} \sum_{\tilde{s}} \mu^{j,i\tilde{\tau}\tilde{s}}_{k|k-1} l^{j,i\tilde{\tau}\tilde{s}}. \tag{31}$$

Note that a missed detection would mean that the likelihood (30) is that of an empty set of measurements. From [15, Sec. V], we have that for the missed detection case

$$w^{j,i}_k = \begin{cases} w^{j,i}_{k|k-1}(1 - r^{j,i}_{k|k-1} + r^{j,i}_{k|k-1} L^{j,i}) \\ \quad \text{for exteroceptive} \\ w^{j,i}_{k|k-1} \quad \text{for target-provided} \end{cases} \tag{32}$$

$$r^{j,i}_k = \begin{cases} \dfrac{r^{j,i}_{k|k-1} L^{j,i}}{1 - r^{j,i}_{k|k-1} + r^{j,i}_{k|k-1} L^{j,i}} & \text{for exteroceptive} \\ r^{j,i}_{k|k-1} & \text{for target-provided} \end{cases} \tag{33}$$

whereas the state density remains unchanged from the prediction, a consequence of the model choice of state-independent detection probability. We distinguish between the two measurement types to highlight how the absence of target-provided information does not impact the weight and existence probability, as it does for the exteroceptive measurements. This is due to how the detection probability (10) is defined. Updating the weights based on a detection is done as

$$w^{j,i}_k = w^{j,i}_{k|k-1}(r^{j,i}_{k|k-1} L^{j,i}). \tag{34}$$

The updated existence probability $r^{j,i}_k$ is 1, and the state density is updated by use of (26)-(29).

C. GLOBAL HYPOTHESES

With the updated Bernoulli components we now need to form global hypotheses and calculate their weights. This is done as described in [36, Sec. C.3], from which we give a summary. For each previous global hypothesis j, we must assign each new measurement to either an existing track or a new track. One such set of assignments amounts to a new global hypothesis. Its weight w_k^j is calculated as the product of the weights of the individual Bernoulli components in the hypothesis. The global hypotheses are formed in the same way for both exteroceptive and target-provided measurements. The number of global hypotheses can quickly become untenable, so rather than considering all possible assignments, we only consider the most likely assignments. These can, for example, be found by use of Murty's method [37] or stochastic optimization [38].

V. APPLICATION TO POINT TARGET TRACKING AND EXTENDED OBJECT TRACKING

We want closed form recursions for the AIS-IMM-PMBM filter and the AIS-GP-PMBM filter. For that purpose, we specify the state spaces, kinematic models, and measurement models for the two filters. We show how the resulting expressions relate to those in Section IV, and that they allow us to perform the calculations by use of Kalman filtering. Furthermore, we show how to estimate the states we want to output to the surrounding system.

A. THE AIS-IMM-PMBM FILTER FOR POINT TARGET TRACKING

For the AIS-IMM-PMBM point target tracker, the hybrid state is

$$\mathbf{y} = \begin{bmatrix} \mathbf{x} & \tau & s \end{bmatrix}^\top \tag{35}$$

in which the kinematic state $\mathbf{x}$ is

$$\mathbf{x} = \begin{bmatrix} x & v_x & y & v_y & \omega \end{bmatrix}^\top. \tag{36}$$

Here, x and y is the position, v_x and v_y are the velocities, and ω is the angular velocity. We have omitted the time index, the global hypothesis index j, and the track index i for brevity. We model the estimated kinematic states, the kinematic state transition, and the measurements as Gaussians distributions. That is, we have that the state density (13) is given by

$$p(\mathbf{y}) = \mathcal{N}(\mathbf{x}; \hat{\mathbf{x}}^{s\tau}, \mathbf{P}^{s\tau}) \mu^{s\tau} \xi^{\tau} \tag{37}$$

where $\hat{\mathbf{x}}^{s\tau}$ and $\mathbf{P}^{s\tau}$ are the estimated mean and covariance conditioned on kinematic model s and ID τ, $\mu^{s\tau}$ is the probability of kinematic model s conditioned on ID τ, and ξ^{τ} is the probability of ID τ.

We use two constant velocity (CV) models and one coordinated turn (CT) model to model the movement of the point targets. The CV models model linear, straight-line motion, whereas the CT model in addition models the possibility of a target turning. In general, the state evolves according to

$$\mathbf{x}_k = \mathbf{F}^s(\mathbf{x}_{k-1})\mathbf{x}_{k-1} + \mathbf{v}_k, \quad \mathbf{v}_k \sim \mathcal{N}(\mathbf{0}, \mathbf{Q}^s). \tag{38}$$

The CV models are defined as

$$\mathbf{F}^{CV} = \begin{bmatrix} 1 & T \\ 0 & 1 \end{bmatrix} \otimes \mathbf{I}_2, \tag{39}$$

$$\mathbf{Q}^{CV} = \begin{bmatrix} (T)^3/3 & (T)^2/2 \\ (T)^2/2 & T \end{bmatrix} \otimes \begin{bmatrix} q_a & 0 \\ 0 & q_a \end{bmatrix}. \tag{40}$$

and the CT model is defined as

$$\mathbf{F}^{CT}(\mathbf{x}_k) = \begin{bmatrix} 1 & 0 & \sin T\omega/\omega & -1+\cos T\omega/\omega & 0 \\ 0 & 1 & 1-\cos T\omega/\omega & \sin T\omega/\omega & 0 \\ 0 & 0 & \cos T\omega & -\sin T\omega & 0 \\ 0 & 0 & \sin T\omega & \cos T\omega & 0 \\ 0 & 0 & 0 & 0 & 1 \end{bmatrix}, \tag{41}$$

$$\mathbf{Q}^{CT} = \begin{bmatrix} \mathbf{Q}^{CV} & \mathbf{0} \\ \mathbf{0} & Tq_\omega \end{bmatrix}. \tag{42}$$

This is a non-linear model, so for use in an extended Kalman filter it is linearized as it is done in [34, Ch. 11.72]. The kinematic state transition density is given by

$$f_{\mathbf{x}}(\mathbf{x}_k|\mathbf{x}_{k-1}, \tau_k, s_k) = \mathcal{N}(\mathbf{x}_k; \mathbf{F}^{s_k\tau}(\mathbf{x}_{k-1}), \mathbf{Q}^{s_k\tau}). \tag{43}$$

Here, $\mathbf{F}^{s_k\tau}(\mathbf{x}_{k-1})$ is the state transition matrix for kinematic model s_k conditioned on ID τ, and $\mathbf{Q}^{s_k,\tau}$ is the process noise covariance matrix. By using (37) and (43) in (19), we get the predicted kinematic states. The Gaussian mixture in (20) can be approximated by use of moment matching.

1) UPDATE WITH RADAR MEASUREMENTS

The radar measurements are modeled as

$$\mathbf{z} = \mathbf{H}_R\mathbf{x} + \mathbf{w}, \quad \mathbf{w} \sim \mathcal{N}(\mathbf{0}, \mathbf{R}_R) \tag{44}$$

where $\mathbf{H}_R$ is the measurement matrix, $\mathbf{R}_R$ is the measurement noise matrix, and $\mathbf{w}$ is the measurement noise. We model the measurement noise as a combination of Cartesian and polar noise

$$\mathbf{R}_R = \mathbf{R}_C + \mathbf{R}_p \tag{45}$$

where $\mathbf{R}_C$ is the Cartesian measurement noise and $\mathbf{R}_p$ is the polar measurement noise, which is converted to Cartesian coordinates with the method from [39]. The Cartesian noise is meant to account for errors from clustering and sensor noise, and the polar noise is meant to account for errors in the range and bearing.

We assume that a set Z of radar measurements contains either one or zero measurements. The measurement likelihood for a single radar measurement is given by

$$f_{\mathbf{z}}(\mathbf{z}|\mathbf{x}, \tau, s) = \mathcal{N}(\mathbf{z}; \mathbf{H}_R\mathbf{x}, \mathbf{R}_R) \tag{46}$$

and the likelihood for a set of radar measurements is given by

$$f_{\mathbf{z}}(Z|\mathbf{x}, \tau, s) = \begin{cases} P_D f_{\mathbf{z}}(\mathbf{z}|\mathbf{x}, \tau, s) & Z = \{\mathbf{z}\} \\ 1 - P_D & Z = \emptyset \end{cases} \tag{47}$$

which is used in (27) and (30) to get a closed-form solution. Note that the case with the empty measurement

set is only relevant for previous potentially detected targets. Furthermore, the radar clutter measurements are modeled as a PPP with constant intensity $\lambda(Z) = N_c/\pi R^2$. Here N_c is the expected number of clutter measurements and R is the radius of the surveillance area.

2) UPDATE WITH AIS MEASUREMENTS

The position and velocity part of the AIS messages are defined as

$$\mathbf{z} = \mathbf{H}_A\mathbf{x} + \mathbf{w}, \quad \mathbf{w} \sim \mathcal{N}(\mathbf{0}, \mathbf{R}_A) \tag{48}$$

where $\mathbf{H}_A$ is the measurement matrix and $\mathbf{R}_A$ is the measurement noise matrix. As for the radar measurements, the noise matrix is a combination of Cartesian and polar noise, but here the Cartesian noise models the error in the position and the polar noise models the error in the velocity. This is because the positional errors are independent on the distance, and derived from GPS data, whereas the velocity is transmitted as a speed and course. The measurement noise matrix is given by

$$\mathbf{R}_A = \mathbf{H}^{\text{pos}}\mathbf{R}_{C,A} + \mathbf{H}^{\text{vel}}\mathbf{R}_{p,A} \tag{49}$$

where pos and vel denote the position and velocity parts of the state, respectively. We use the same method as above when we convert the polar noise matrix to Cartesian coordinates.

For the position- and velocity-information in the AIS messages, the measurement likelihood $f_{\mathbf{p}}^{tp}(\mathbf{p}|\mathbf{y})$ in (11) is given by

$$f_{\mathbf{p}}^{tp}(\mathbf{p}|\mathbf{y}) = \mathcal{N}(\mathbf{z}; \mathbf{H}_A\mathbf{x}, \mathbf{R}_A). \tag{50}$$

Furthermore, we utilize the ID information in the AIS messages. We account for the small possibility of the ID provided by the measurement is incorrect, relative to the actual ID of the target, by use of a probability P_C representing our confidence in the ID provided by the measurement being correct. The likelihood of the ID only depends on the ID of the target. We formulate $f_{\tau}^{tp}(\tau^{\mathbf{z}}|\mathbf{y}_k)$ as

$$f_{\tau}(\tau^{\mathbf{z}}|\tau) = \begin{cases} P_C & \text{if } \tau = \tau^{\mathbf{z}} \\ \dfrac{1-P_C}{|\mathcal{V}|-1} & \text{if } \tau \neq \tau^{\mathbf{z}} \text{ and } \tau > 0 \\ 0 & \text{if } \tau = 0 \end{cases} \tag{51}$$

where $\tau^{\mathbf{z}}$ is the ID provided by the measurement. A zero-valued ID τ is used to represent a target that does not transmit any information, and as such has no observable ID. We combine (50) and (51) in (11), and disregard the length- and width-related terms in the latter equation. This provides a closed form solution to the integral in (30), and furthermore allows us to calculate the updated kinematic states in (27) by use of the Kalman filter equations.

B. THE AIS-GP-PMBM FILTER FOR EXTENDED OBJECT TRACKING

The hybrid state in the AIS-GP-PMBM filter is

$$\mathbf{y} = \begin{bmatrix} \mathbf{x} & \tau & \alpha & \beta \end{bmatrix}^\top \tag{52}$$

and includes the ID τ and two gamma distribution shape parameters α and β. The gamma distribution is used to estimate the expected number of detections from a target. Furthermore, $\mathbf{x}$ is given by

$$\mathbf{x} = \begin{bmatrix} x & v_x & y & v_y & \phi & \omega & \mathbf{x}^f \end{bmatrix}^\top. \tag{53}$$

Here, ϕ is the target heading, ω is the angular velocity, and $\mathbf{x}^f$ is a vector which parametrizes the contour of the target extent, specifically it contains the values of a radius function f at equidistant angles. The single state estimates are represented as gamma-Gaussian distributions on the form

$$p(\mathbf{y}) = \mathcal{N}(\mathbf{x}; \hat{\mathbf{x}}^\tau, \mathbf{P}^\tau)\mathcal{G}(\alpha, \beta)\xi^\tau \tag{54}$$

where we again have omitted the time index, the track index i, and the global hypothesis index j for brevity. For the augmented state in the AIS-GP-PMBM filter, we combine the CV model with a process model for the extent. In addition to linear velocity, the CV model also models the heading and angular velocity, and is defined as

$$\mathbf{F}^{CV} = \begin{bmatrix} 1 & T \\ 0 & 1 \end{bmatrix} \otimes \mathbf{I}_3 \tag{55}$$

$$\mathbf{Q}^{CV} = \begin{bmatrix} (T)^3/3 & (T)^2/2 \\ (T)^2/2 & T \end{bmatrix} \otimes \begin{bmatrix} q_a & 0 & 0 \\ 0 & q_a & 0 \\ 0 & 0 & q_\theta \end{bmatrix}. \tag{56}$$

We have that $\mathbf{F} = diag(\mathbf{F}^{CV}, \mathbf{F}^f)$ and $\mathbf{Q} = diag(\mathbf{Q}^{CV}, \mathbf{Q}^f)$ where

$$\begin{aligned} \mathbf{F}^f &= \exp(-\Delta t \eta_\gamma)\mathbf{I}, \\ \mathbf{Q}^f &= (1 - \exp(-2\Delta t \eta_\gamma))\mathbf{K}(\Theta^f, \Theta^f). \end{aligned} \tag{57}$$

$\mathbf{K}(\Theta^f, \Theta^f)$ is the covariance matrix of the Gaussian process, and Θ^f contains the angles of the points which define the extent. For further details, we refer to [27] for the derivation of the Gaussian process model, or to [6] for a shorter summary.

When predicting and updating the single state estimates, conditioned on their IDs, we separate the gamma and Gaussian parts of the distributions. This allows us to use the Kalman filter equations to calculate the predicted and updated Gaussian parts the same way as in Section V-A, whereas the variables in the gamma distribution are predicted as

$$\alpha_{k|k-1} = \alpha_{k-1}/\eta_\gamma, \quad \beta_{k|k-1} = \beta_{k-1}/\eta_\gamma \tag{58}$$

and updated as

$$\alpha_k = \alpha_{k|k-1} + |Z|, \quad \beta_k = \beta_{k|k-1} + 1. \tag{59}$$

Here, η_γ is called the forgetting factor and is a parameter that controls how quickly the measurements received in the past should be forgotten by the gamma distribution parameters.

1) UPDATE WITH LIDAR MEASUREMENTS

A generic measurement equation for one contour generated measurement with the target contour parametrized by a radial function f can be written as

$$\mathbf{z}^l = \mathbf{x}^c + \mathbf{p}(\theta^l)f(\theta^l) + \mathbf{w}^l$$

$$\mathbf{p}(\theta^l) = \begin{bmatrix} \cos\theta^l \\ \sin\theta^l \end{bmatrix} \tag{60}$$

where $\mathbf{z}_k^l$ is measurement l and θ^l is the corresponding angle of the origin of the measurement of the target contour. θ^l can be expressed both in a global frame $\theta^{l(G)}$ and the local target body frame $\theta^{l(B)}$ as

$$\begin{aligned} \theta^{l(B)}(\mathbf{x}^c, \phi) &= \theta^{l(G)}(\mathbf{x}^c) - \phi \\ \theta^{l(G)}(\mathbf{x}^c) &= \angle\left(\mathbf{z}^l - \mathbf{x}^c\right) \end{aligned} \tag{61}$$

The value of $f(\theta^l)$ can be found by calculating the value of the matrix $\mathbf{H}^{(f)}$ for the specific angle using Gaussian process regression and multiplying it with the vector parametrizing the extent $\mathbf{x}^f$. Therefore, the measurement equation can be written as

$$\begin{aligned} \mathbf{z}^l &= \mathbf{x}^c + \mathbf{p}^l(\theta^{l(G)}(\mathbf{x}^c))\mathbf{H}^{(f)}\left(\theta^{l(B)}(\mathbf{x}^c, \phi)\right)\mathbf{x}^f + \mathbf{w}^l \\ &= h^l(\mathbf{x}) + \mathbf{w}^l, \qquad \mathbf{w}^l \sim \mathcal{N}(\mathbf{0}, \mathbf{R}^l). \end{aligned} \tag{62}$$

The measurement equation is therefore dependent on the state space components $\mathbf{x}^c$, ϕ and $\mathbf{x}^f$, of which the two former are non-linear terms in the measurement equation. It should be noted that this is an implicit equation, due to the dependency of $\theta^{l(G)}$ on $\mathbf{z}^l$. Similarly, the estimated error of the Gaussian process regression can be calculated by calculating a matrix $\mathbf{R}^f$ and by projecting this into 2D we get

$$\mathbf{R}^l = \mathbf{p}^l(\mathbf{x}^c)\mathbf{R}^f\left(\theta^{l(B)}(\mathbf{x}^c, \phi)\right)\mathbf{p}^l(\mathbf{x}^c)^T + \mathbf{R}_C. \tag{63}$$

We use an iterated extended Kalman filter to deal with the non-linearities that are introduced by the LiDAR measurement model.

A global association hypothesis in extended object tracking does not assign each measurement to a single potential target, but rather assigns sets of measurements to potential targets. The measurement likelihood for a single measurement can thus be written as

$$f_{\mathbf{z}}(\mathbf{z}^l|\mathbf{x}) = N(\mathbf{H}^l\mathbf{x}, \mathbf{R}^l). \tag{64}$$

Each potential target i is associated to a specific measurement cell C and the measurements in such a cell is denoted Z_C. The measurement set likelihood is given by the following inhomogeneous PPP [5]

$$f_{\mathbf{z}}(Z_C|\mathbf{x}) = \exp(-\lambda_m)\lambda_m^{|Z_C|}\prod_{\mathbf{z}^l \in Z_C} f_{\mathbf{z}}(\mathbf{z}^l|\mathbf{x}) \tag{65}$$

here λ_m is the Poisson rate governing the expected number of measurements, which is estimated by the gamma distribution, i.e. $\lambda_m \sim \mathcal{G}(\alpha, \beta)$. Given this, the predictive likelihood can be calculated as in (30), which results in

$$l^\tau = P_D\frac{\Gamma(\alpha + |Z_C|)\beta^\alpha}{\Gamma(\alpha)(\beta+1)^{(\alpha+|Z_C|)}|Z_C|!}\prod_{\mathbf{z}^l \in Z_C}\mathcal{N}(\mathbf{z}^l; \mathbf{H}^l\hat{\mathbf{x}}^{\tau,l}, \mathbf{S}^{\tau,l}) \tag{66}$$

where $\mathbf{S}^{\tau,l}$ is the innovation covariance matrix for measurement l conditioned on ID τ. If the measurement cell is empty, the predictive likelihood is instead given by the effective probability of missed detection defined by

$$l^\tau = 1 - P_D + P_D\exp(\lambda_m) \tag{67}$$

which represents the fact that we can have a missed detection either due to the probability of detection or the probability that the target is detected but generates zero measurements. Lastly, as for the radar measurements, we assume that the clutter intensity is uniform over the surveillance area. Furthermore, the intensity also reflects the result that a cell with more than one measurement never is a false alarm. This means that

$$\lambda(Z_C) = \begin{cases} N_c/\pi R^2 & |Z_C| = 1 \\ 0 & |Z_C| > 1. \end{cases} \tag{68}$$

Further details regarding the Gaussian process PMBM filter can be found in [6].

2) UPDATE WITH AIS MEASUREMENTS

The incoming target-provided measurements are handled in a similar manner as for the point target tracking case, as they uphold the assumption of each target only providing a single measurement. The difference is that we now include the dimensions of the target in the measurement vector. The dimension is modeled by considering length and width separately. The measurement model matrix can be found using Gaussian process regression, in this case by using fixed angles which correspond to the length

$$z^L = \mathbf{H}^{(f)}(0)\mathbf{x}^f + \mathbf{H}^{(f)}(\pi)\mathbf{x}^f + w^L, \qquad w^L \sim \mathcal{N}(0, \sigma_{z,L}^2) \tag{69}$$

and width

$$\begin{aligned} z^W &= \mathbf{H}^{(f)}\left(\frac{\pi}{2}\right)\mathbf{x}^f + \mathbf{H}^{(f)}\left(\frac{3\pi}{2}\right)\mathbf{x}^f + w^W, \\ w^W &\sim \mathcal{N}(0, \sigma_{z,W}^2). \end{aligned} \tag{70}$$

The estimated measurement noise covariance has a component for Gaussian process regression, and is given by

$$\begin{aligned} \sigma_L^2 &= \mathbf{R}^{(f)}(0) + \mathbf{R}^{(f)}(\pi) + \sigma_{z,L}^2 \\ \sigma_W^2 &= \mathbf{R}^{(f)}\left(\frac{\pi}{2}\right) + \mathbf{R}^{(f)}\left(\frac{3\pi}{2}\right) + \sigma_{z,W}^2. \end{aligned} \tag{71}$$

Using this, we get that the AIS measurement likelihood (11) becomes

$$\begin{aligned} f_{\mathbf{z}}(Z|\mathbf{y}) = f_\tau(\tau^{\mathbf{z}}|\tau)&\mathcal{N}(\mathbf{p}; \mathbf{H}\mathbf{x}^c, \mathbf{R}^c)\times \\ &\mathcal{N}(z^L; \mathbf{H}^{(f)}(0)\mathbf{x}^f + \mathbf{H}^{(f)}(\pi)\mathbf{x}^f, \sigma_L^2)\times \\ &\mathcal{N}(z^W; \mathbf{H}^{(f)}\left(\frac{\pi}{2}\right)\mathbf{x}^f + \mathbf{H}^{(f)}\left(\frac{3\pi}{2}\right)\mathbf{x}^f, \sigma_W^2) \end{aligned} \tag{72}$$

when $Z = \{\mathbf{z} = [\mathbf{p}, \tau, z^L, z^W]\}$. This is used in (27) and (30). The gamma distribution is only concerned with the exteroceptive measurements and is as such not updated when target-provided measurements are received because no new

information is received. It is also ignored when calculating the target-provided measurement likelihoods.

Remark. *Note that we do not use multiple models in the extended object AIS-GP-PMBM. This is equivalent to having a single model with constant probability* 1*, and the simplified expressions are easily derived from the ones in Sections IV-A and IV-B.*

C. STATE ESTIMATION AND COMPLEXITY MANAGEMENT

The implementation for the point target tracker largely follows [36], whereas the extended object tracker is based on [5]. The way we perform state estimation and manage the computational complexity is, however, conceptually the same. After each update step we have several global hypotheses, each containing Bernoulli components representing potentially detected targets. In [36] three estimation methods are presented, which allows us to choose which of the large number of possible target states we decide are the most likely. For both point targets and extended objects, we use the first of the three methods, which simply decides upon the global hypothesis with the highest weight. Of the Bernoulli components in the chosen global hypothesis, all with an existence probability larger than some threshold T_r are selected as the output. Furthermore, each state estimate is a Gaussian mixture with weights corresponding to the probabilities of the discrete states, such as IDs. A single Gaussian is extracted by use of moment matching.

Even when limiting the amount of new global hypotheses, with Murty's algorithm for point targets and stochastic optimization for extended objects, the number of Bernoulli components can become very large. Thus, to avoid an unmanageable number of possible target states some approximations are made. First, we limit the amount of Bernoulli components created at each time step by way of gating the measurements. This is done by only considering the measurements less than $\sqrt{g}$ standard deviations from a given prediction. Thus, new potential targets are only created for measurements close enough to an unknown target, and already potentially detected targets are only updated based on the measurements within its gate area.

Furthermore, we do not propagate all Bernoulli components from each time step to the next. We follow the strategy from [36], and only keep the N_{hyp} global hypotheses with highest weights. In addition, we remove all Bernoulli components with existence probability lower than some threshold T_b and those not present in any of the kept global hypotheses. Furthermore, we only keep the Poisson densities with weight higher than T_p. A brief description covering one iteration of the AIS-PMBM is given in Algorithm 1.

Algorithm 1 An Iteration of the AIS-PMBM

Input: Previous unknown target densities $\mu(\mathbf{y})$, potentially detected target densities $p^{i,j}(\mathbf{y})$, global hypotheses, and new measurements Z

Output: Updated unknown target densities $\mu(\mathbf{y})$, potentially detected target densities $p^{i,j}(\mathbf{y})$, global hypotheses

1: Predict unknown target densities with (14) and perform gating.
2: Initialize new potentially detected targets on the gated measurements with the expressions from Section IV-B1.
3: Predict potentially detected targets with (16)-(19) and perform gating.
4: Initialize new Bernoulli components for the previously potentially detected targets with the expressions from Section IV-B2.
5: Find new global hypotheses based on the previous global hypotheses and the new Bernoulli components as described in Section IV-C.
6: Output the Bernoulli components in the best global hypothesis with existence probability higher than T_r.
7: Remove all but the N_{hyp} best global hypotheses, prune Bernoulli components with low existence probability, and prune Poisson densities with low weight.

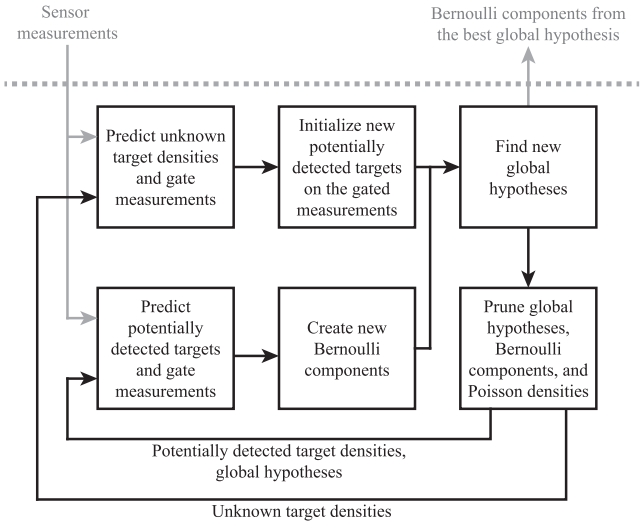

FIGURE 1. A flow chart describing the program flow of the AIS-PMBM algorithm, as described in Algorithm 1.

VI. RESULTS FOR POINT TARGET TRACKING

To evaluate the performance of the trackers we use the GOSPA metric for trajectories, presented in [40]. The metric works on sets of trajectories, and penalizes track switches in addition to localization errors, false alarms, and missed detections. It also allows us to look at the different error sources in isolation, highlighting the advantages and shortcomings of different methods. The metric is defined as

$$d_p^{(c,\gamma)}(X,Y) \triangleq \min_{\substack{a_k \in \prod_{k=1,\dots,T}^{X,Y}}} \left(\sum_{k=1}^{T} d_k^{X,Y}(X,Y,a_k)^p) + \sum_{k=1}^{T-1} s^{X,Y}(a_k,a_{k+1})^p \right)^{\frac{1}{p}} \tag{73}$$

where the first sum penalizes localization errors and cardinality errors, and the second sum the track switch error. a_k is one of the possible associations at time k between the sets of trajectories X and Y. In our case, the sets of trajectories are the true trajectories and the target states estimated as described in Section V-C. The continuity of the estimated target states is based on their originating measurement. The parameters of the metric are the order p, the cutoff c, and the switch penalty γ. The cutoff decides the point where the distance between two tracks is too large to be considered a feasible association. We have that

$$d_k^{X,Y}(X, Y, a_k)^p \triangleq \sum_{(i,j)\in\theta_k(a_k)} d(\mathbf{x}_k^i, \mathbf{y}_k^i)^p + \frac{c^p}{2}(|\tau_k(X)| + |\tau_k(Y)| - 2|\theta_k(a_k)|). \tag{74}$$

Here, $d(\cdot, \cdot)$ is the distance function, $\theta_k(\cdot)$ is the set of feasible associations in the kth time step, and $\tau_k(\cdot)$ is the set of elements in a set of trajectories at time step k. The track switch error is defined as

$$s^{X,Y}(a_k, a_{k+1})^p \triangleq \gamma^p \sum_{i=1}^{n_X} s(a_k^i, a_{k+1}^i) \tag{75}$$

where $s(\cdot, \cdot)$ is 0 if the association between the trajectories is unchanged, 1 if the association is changed to a different trajectory, and $1/2$ if the association is changed and the trajectory is now unassigned, or was previously unassigned. We use the implementation available at [41] to perform the computations, and only compute errors at the time steps where exteroceptive measurements have been received.

A. SIMULATED DATA

We test seven different trackers and tracker configurations. These are

1) The MHT algorithm with AIS from [32].
2) The PMBM with AIS of Miao et al. [14].
3) The AIS-VIMMJIPDA from [15].
4) The PMBM operating only on the radar measurements.
5) The IMM-PMBM operating only on the radar measurements.
6) The AIS-PMBM.
7) The AIS-IMM-PMBM.

The trackers are tested on two different types of simulated data sets. The first of these is a data set configuration described in [2]. The data sets consider several targets that are all situated approximately at the origin of the area halfway through the simulation. The scenario is created by first choosing the points where the targets are to meet, and then stepping backwards and forwards with some kinematic model to create their trajectories. For the purposes of our simulations, we consider ten targets, whose midpoint positions and velocities are drawn from $\mathcal{N}(\mathbf{0}, 0.25 \times \mathbf{I})$, the same as for Case 2 in [2]. The radar and AIS measurements are generated according to the measurement models described in Section V, with the frequency of the AIS measurements decided by the requirements set by the protocol [10].

Furthermore, the different PMBM variants are tested on the Ravens data set detailed in [4]. The data set is designed to pose a challenge to the trackers and consists of eight targets and one ownship. During a span of 23 minutes, the targets and the ownship move in formation, making maneuvers underway. For the data to be suitable for testing of fusion between radar and AIS, additional AIS measurements are created for six of the eight targets.

The tuning parameters are shown in Table 1 for all the trackers. For the AIS-PMBM from Miao et al., we calculate the AIS detection probability directly from the total number of AIS messages received, together with the number of targets present in the area and their life span. Furthermore, the Cartesian noise component in the AIS measurement noise is increased to 10^2 to account for the time difference between transmission and processing of the measurements. Also note that the MHT algorithm does not implement the measurement noise with a polar component, and thus only uses Cartesian measurement noise. The process noise and initial model probabilities of the PMBM and JIPDA trackers differ, in the case of the initial mode probabilities significantly. During simulations, it became evident that the PMBM trackers needed more process noise than the JIPDA tracker to follow the targets successfully. This can be due to the step where the JIPDA combines the track-to-measurement associations, which has the observed effect of somewhat averaging the individual target movements across closely spaced targets.

1) RESULTS

Results for the first data sets, with targets that meet in the middle of the surveillance area, are shown in Figure 2 and Table 2. Overall, the plots show that the most difficult parts of the scenario are at the very start, the middle, and at the very end. Most trackers perform best in the intervening periods. That the trackers struggle at the midpoint is no surprise, as all targets are closely spaced. Furthermore, as the targets are initialized with relatively low velocities and evolve from the midpoint, they usually have higher velocities at the start and end points. This means that they are harder to track correctly, and errors caused by delays in initialization and termination of tracks also contribute to the observed effect.

Next, we look at the performance of the different trackers relative to each other. It is evident that the MHT algorithm struggles more than the other trackers, especially with initializing tracks on all targets. Furthermore, the AIS-VIMMJIPDA performs well in many aspects but struggles in the middle of the scenario. These struggles manifest themselves in both false alarms, and missed detections which are present almost to the end of the scenario. Its IMM capabilities does, however, result in a low localization error, perhaps helped by the fact that the most troublesome targets are not tracked. For the different PMBM variants, the results

TABLE 1. Tuning parameters for the point target scenarios. If the parameters differ between the two scenarios, they are listed with the parameter for the first scenario first, and for the second scenario last.

Quantity	Symbol Unit	Value (1st, 2nd)
Common parameters		
Survival probability	P_{S} $[-]$	0.999
Gate size	g $[-]$	20
Max. number of hypotheses	$N_{\max}$ $[-]$	400
Area radius	R [m]	1000, 100
Clutter intensity	λ $[\mathrm{m}^{-2}]$	$4/(\pi R^2)$
Initial velocity std.	σ_v $[\mathrm{m\,s}^{-1}]$	10
Existence confirmation threshold	T_c $[-]$	0.99
Radar measurements		
Cartesian noise std.	σ_{c_R} [m]	1.0
Polar range std.	σ_r [m]	2.0
Polar bearing std.	σ_θ [°]	2
Detection probability	P_{D} $[-]$	0.9
AIS measurements		
Cartesian noise std.	σ_{c_R} [m]	1.0
Polar range std.	σ_r [m]	2.0
Polar bearing std.	σ_θ [°]	2
Confidence probability	P_C $[-]$	0.999
Unknown target no ID probability	ξ_u^0 $[-]$	0.9
PMBM parameters		
Poisson pruning threshold	T_{Pp} $[-]$	1.0×10^{-5}
Bernoulli component pruning threshold	T_{Bp} $[-]$	1.0×10^{-6}
Birth weight	U $[\mathrm{m}^{-2}]$	1×10^{-3}
CV model 1 process noise intensity	$q_{a,1}$ $[\mathrm{m}^2\,\mathrm{s}^{-3}]$	0.2^2
CV model 2 process noise intensity	$q_{a,2}$ $[\mathrm{m}^2\,\mathrm{s}^{-3}]$	2^2
Turn rate process noise intensity	q_ω $[\mathrm{rad}^2\,\mathrm{s}^{-3}]$	0.002^2
Single model process noise intensity	$q_{a,1}$ $[\mathrm{m}^2\,\mathrm{s}^{-3}]$	0.8^2
Initial model probability	μ_u^s [%]	$\begin{bmatrix}25 & 25 & 50\end{bmatrix}$
IMM transition probability	$\pi^{\tilde{s}s}$ [%]	$\begin{bmatrix}99 & .5 & .5\\ .5 & 99 & .5\\ .5 & .5 & 99\end{bmatrix}$
JIPDA parameters		
Existence termination threshold	T_d $[-]$	1.0×10^{-5}
CV model 1 process noise intensity	$q_{a,1}$ $[\mathrm{m}^2\,\mathrm{s}^{-3}]$	0.1^2
CV model 2 process noise intensity	$q_{a,2}$ $[\mathrm{m}^2\,\mathrm{s}^{-3}]$	1.5^2
Turn rate process noise intensity	q_ω $[\mathrm{rad}^2\,\mathrm{s}^{-3}]$	0.15^2
Initial existence probability	r_u [-]	0.18
Initial visibility probability	η_u [-]	0.9
Visibility transition probability	$\pi^{\tilde{s}s}$ [%]	$\begin{bmatrix}48 & 52\\ 10 & 90\end{bmatrix}$
Initial model probability	μ_u^s [%]	$\begin{bmatrix}80 & 10 & 10\end{bmatrix}$
MHT parameters		
Number of tailed time steps	N $[-]$	5
Initialization window size	N_M $[-]$	5
Measurements needed for initialization	M $[-]$	2
Birth rate	U $[\mathrm{m}^{-2}]$	1×10^{-3}
Cartesian noise std.	σ_{c_R} [m]	4.0
Process noise intensity	q $[\mathrm{m}^2\,\mathrm{s}^{-3}]$	1.0^2
Initial velocity std.	σ_v $[\mathrm{m\,s}^{-1}]$	20
Similar track prune threshold	T_{STP} $[-]$	0

show that both IMM and use of AIS measurements reduce the GOSPA value. The pure PMBM tracker outperforms the two previously mentioned trackers, albeit with regards to the AIS-VIMMJIPDA tracker by only a slight margin. Furthermore, all its augmentations perform even better. When including the AIS measurements, the general trend across the different trackers is an improvement in all error sources except for the false alarms. Because tracks initialized on AIS measurements get a higher weight than those initialized on radar measurements, this is somewhat expected. On the other hand, the use of AIS noticeably decreases the number of missed detections. Regarding the PMBM variant from [14], its performance lands between that of the regular PMBM and the AIS-PMBM presented here. This can be explained by the fact that the AIS messages are limited by a low P_D, thus giving them reduced influence on the results in comparison to the AIS-PMBM presented here. Increasing the P_D, however, could result in premature terminations when AIS messages are not available. Furthermore, we see that use of IMM improves performance noticeably for all error sources except the false alarms, where we see a slight increase.

For the Ravens data set we only consider the four different PMBM variants. The results are shown in Figure 3 and Table 3, and show the same trend as we saw in the previous data with more advanced methods performing better overall. There are, however, some interesting idiosyncrasies. The trackers with IMM provide better localization estimates than their counterparts before the midway point but worse after. At the very end of the scenario this can be explained with the non-IMM trackers losing track of their targets, and thus the localization error of the more difficult targets is not included. This does not, however, explain why this also occurs before the track losses happen. An explanation can be that we experience a trade-off between precise estimation of individual targets and being able to track all targets. That is, to be able to handle large changes in acceleration the added covariance in the prediction is often too large when the targets do not perform challenging maneuvers. Even though the IMM framework should be able to account for this, it may struggle to estimate the mode probabilities correctly due to the challenging scenario. Nevertheless, the differences between methods are not large, and the IMM methods perform better by the total GOPSA metric. Furthermore, this indicates that looking only at single components of the GOSPA metric will not give a complete picture of the performance of the trackers.

B. EXPERIMENTAL VALIDATION IN A CLOSED-LOOP EXPERIMENT

The AIS-IMM-PMBM was also used during the testing of an autonomous surface vehicle (ASV) in the Trondheimsfjord in October 2023. A more extensive description of the testing and additional scenarios is available at [42]. In the context of this paper, the purpose of using the AIS-IMM-PMBM method in the experiment was to demonstrate the feasibility

TABLE 2. GOSPA-T values for the different tracker configurations when tested on the data set configuration from [2], corresponding to the averaged values in Figure 3. The best result for each error source is highlighted in bold.

	PMBM	AIS-PMBM	IMM-PMBM	AIS-IMM-PMBM	AIS-PMBM from Miao et al.	AIS-VIMMJIPDA	MHT
Total GOSPA	10.424	9.964	8.809	**8.465**	10.111	13.211	27.013
Localization	9.107	8.718	7.943	**7.520**	8.702	9.341	12.300
Missed detection	1.013	0.739	0.511	**0.482**	1.185	4.649	15.852
False alarm	0.238	0.328	0.262	0.344	**0.206**	0.482	4.961
Track switch	1.055	1.140	0.732	0.755	0.962	**0.670**	1.513

TABLE 3. GOSPA-T values for the different PMBM configurations when tested on the Ravens data set, corresponding to the averaged values in Figure 3. The best result for each error source is highlighted in bold.

	PMBM	AIS-PMBM	IMM-PMBM	AIS-IMM-PMBM
Total GOSPA	10.149	8.859	8.151	**6.845**
Localization	6.956	**6.145**	7.280	6.274
Missed detection	3.853	3.556	0.861	**0.670**
False alarm	0.555	0.279	0.292	**0.123**
Track switch	0.446	**0.175**	0.687	0.246

of using an advanced tracker in a larger system with higher demands regarding latency, and to show that it works together with a collision avoidance system. The ASV was equipped with a radar and an AIS receiver. The collision avoidance algorithm, a scenario-based model predictive control method described in [11], was responsible for maneuvering the ASV to avoid collisions with the targets based on input from the AIS-IMM-PMBM.

The scenario involves the ownship, a Mariner from Maritime Robotics, and Juggernaut, a motorboat. The boats are shown in Figure 4. The motorboat was operated by a human operator, and the ownship was tasked with avoiding collisions with the target while maintaining a course towards a waypoint. The scenario was designed to challenge the collision avoidance algorithm, and for it to properly respond to the movements of the target it needed accurate target estimates. What amounts to accurate estimates in this use case is somewhat different from what is usually considered when evaluating target trackers. The course and speed estimates are very important as they are used to predict the future positions of the targets. The position of the target, however, is not as important because the collision avoidance algorithm does not mainly act based on the current target position, but rather on the predicted future positions. An inaccurate course estimate will then have a larger impact than an inaccurate position estimate.

1) RESULTS

The scenario is depicted in Figure 5. The Mariner was tasked with moving on a north-eastern course while the motorboat made several maneuvers that demanded action from the Mariner. The target deliberately acted counter to collision avoidance guidelines, so that the collision avoidance algorithm was forced to make evasive maneuvers. Nevertheless, the AIS-IMM-PMBM tracker was able to provide accurate estimates of the target, and the collision avoidance algorithm was able to respond to the maneuvers. The course and speed estimates are stable and with relatively low uncertainty. Jittery and uncertain estimates would demand greater caution on the part of the collision avoidance algorithm, and it could create situations where the ownship path would have to be recalculated at a higher frequency than necessary. Furthermore, any false alarms were avoided, partly helped by the low clutter density.

The data collected during the scenario was also input to an IPDA tracker, see Figure 6. This was the tracker used in [43], and whereas it is able to track the target its course and speed estimates are considerably noisier than for the AIS-IMM-PMBM. The standard deviations are also larger: for the IPDA the standard deviations are 0.36 knots for the speed and 34.45 degrees for the course, whereas they are 0.25 knots and 15.63 degrees for the speed and course estimated by the PMBM. Because the IPDA uses only a single kinematic model, and furthermore does not use the AIS messages, this is to be expected. However, as the collision avoidance method was not used together with the IPDA, it is difficult to say how this would impact operations. Previous work on use of PDA in radar-based maritime collision avoidance [44] indicates that additional filtering of the speed and course estimates is needed for successful operation. Furthermore, the IPDA is well suited for such a single-target scenario but lacks the flexibility of a more advanced method regarding multiple targets with different movement characteristics.

VII. RESULTS FOR EXTENDED OBJECT TRACKING

For the AIS-GP-PMBM we also use GOSPA for trajectories to evaluate the performance with regards to the position and velocities of the target estimates. Additionally, we need a method to evaluate the extent estimates. For this purpose, we use the intersection-over-union (IOU) between the estimated and true extents of the targets. IOU is found by taking the true extent of the target as the area $\mathcal{E}$ and the estimated extent as the area $\hat{\mathcal{E}}$, which we then use to calculate

$$IOU = \frac{\mathcal{E} \cap \hat{\mathcal{E}}}{\mathcal{E} \cup \hat{\mathcal{E}}}. \tag{76}$$

To pair the correct estimate with the correct ground truth, we use the same assignment procedure that is used when calculating the GOSPA metric. We consider two scenarios that highlight two key challenges that make estimation based on exteroceptive measurements difficult: occlusion and

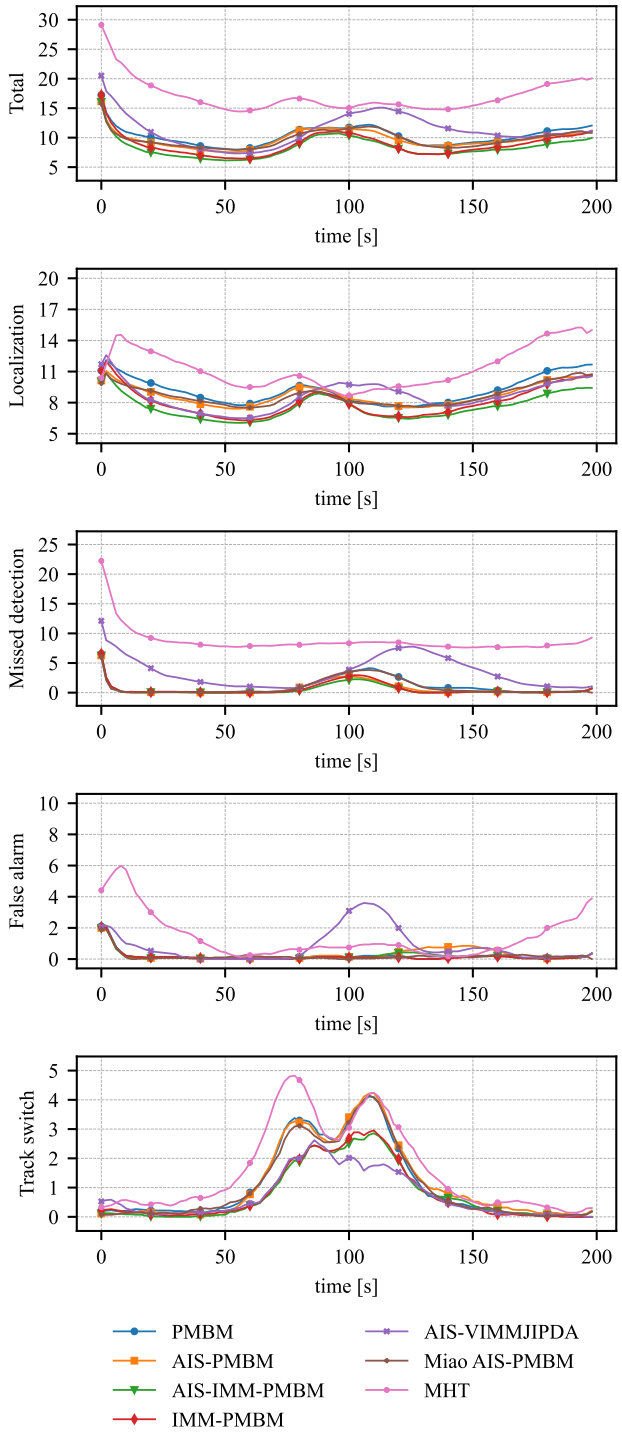

FIGURE 2. GOSPA-T values for the different trackers and configurations, where we see how the different trackers perform for different error sources evolve for the duration of the scenarios. We use the GOSPA parameters $p = 2$, $c = 40$, and $\gamma = 5$. Shown, from top to bottom, is the combined GOSPA-T, the localization error, the missed detection error the false alarm error, and the track switch penalty. For visual clarity the values are plotted as the moving average over 10 time steps.

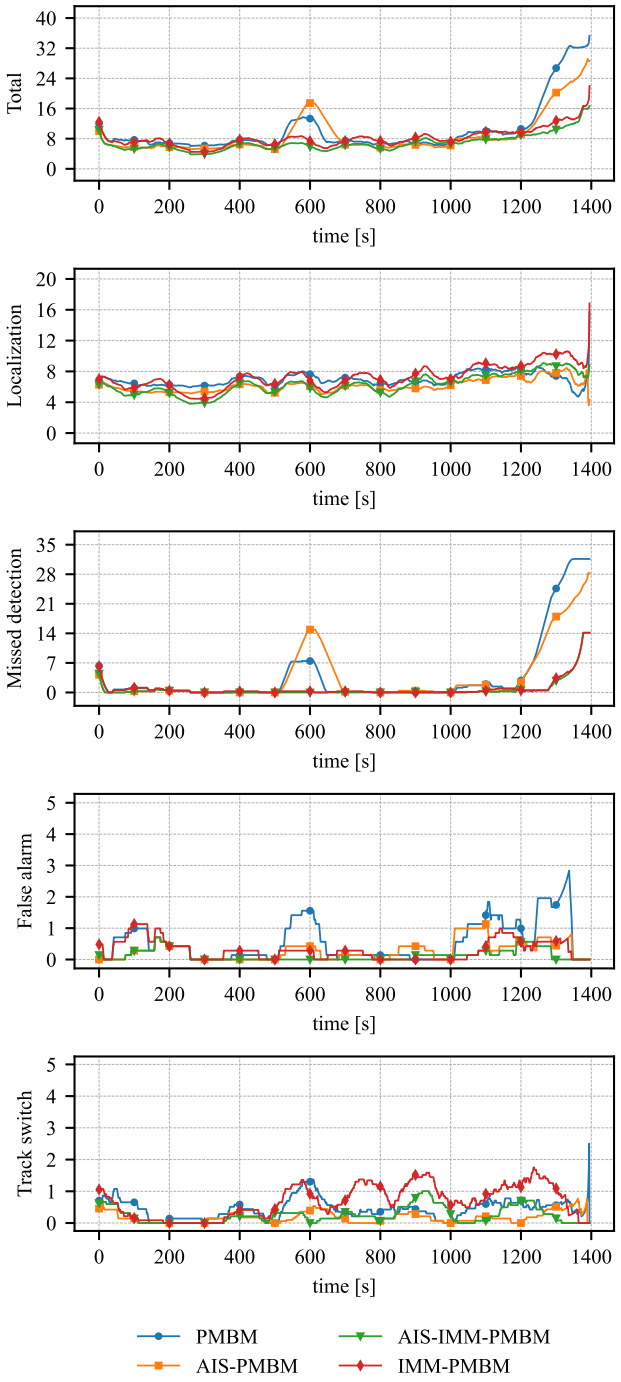

FIGURE 3. GOSPA-T values for the different PMBM tracker configurations. We use the GOSPA parameters $p = 2$, $c = 20$, and $\gamma = 5$. Shown, from top to bottom, is the combined GOSPA-T, the localization error, the missed detection error the false alarm error, and the track switch penalty. The values are from the whole duration of the Ravens data set, and for visual clarity plotted values are the moving average over 100 time steps.

clutter measurements. To properly handle occluded targets is difficult, and the lack of measurements will in most cases result in reduced estimate quality. The clutter model we use is quite simple and assumes that the clutter measurements are uniformly distributed among the sensor cells. As the experimental data demonstrates, this is not necessarily the case, and especially target-dependent clutter, such as that originating from wakes, is difficult to handle. Both these problems are in some ways mitigated when performing point target tracking, as the sensor detections are clustered

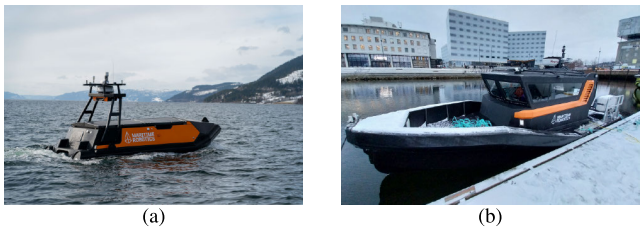

(a) (b)

FIGURE 4. The two ships used in the experimental validation: Mariner (a) and Juggernaut (b). Photos: Maritime Robotics.

TABLE 4. Tuning parameters for the extended object scenarios. If the parameters differ between the two scenarios, they are listed with the parameter for the first scenario first, and for the second scenario last. Any parameters not listed here are identical to ones found in [6].

Quantity	Symbol Unit	Value
Survival probability	P_{S} $[-]$	0.999
Gate size	g $[-]$	20
Max. number of hypotheses	$N_{\max}$ $[-]$	20
Poisson pruning threshold	T_{Pp} $[-]$	1.0×10^{-5}, 1.0×10^{-2}
Bernoulli component pruning threshold	T_{Bp} $[-]$	1.0×10^{-5}, 1.0×10^{-2}
Area radius	R [m]	100, 60
Clutter rate	N_c $[-]$	16, 80
Initial velocity std.	σ_v [m s^{-1}]	3
Initial heading std.	σ_ψ [°]	180
Initial ang. vel. std.	σ_ω [° s^{-1}]	45
Existence confirmation threshold	T_c $[-]$	0.99
Motion noise intensity	q_a [m^2 s^{-3}]	0.2^2
Heading noise intensity	q_θ [°]	0.1^2, 0.3^2
Number of birth components	N_b $[-]$	36
Birth weight	U [m^{-2}]	$1/36$
Forgetting factor	η_γ $[-]$	0.99
Gamma distribution shape parameters	α, β $[-]$	$[1000\ 100]$, $[500\ 100]$
Lidar measurements		
Detection probability	P_D $[-]$	0.9
Cartesian noise std.	σ_r [m]	0.1, 0.5
AIS measurements		
Cartesian noise std.	σ_{c_R} [m]	1.0
Polar range std.	σ_r [m]	1.0
Polar bearing std.	σ_θ [°]	10
Confidence probability	P_C $[-]$	0.999
Unknown target no ID probability	ξ_u^0 $[-]$	0.9
Length and width std.	$\sigma_{l,w}$ [m]	0.5

before they are input to the tracker. This means that partial occlusions will not necessarily result in loss of measurements, and that target-dependent clutter can be clustered together with target detections. For extended object tracking, however, we do not have these advantages.

The tuning parameters for both scenarios are shown in Table 4.

A. SIMULATED DATA

The simulated data used to evaluate the EOT methods is the same as that used in [6]. It consists of four targets, with a LiDAR located at the center of a surveillance area with a 100-meter radius. As for the Ravens data set, AIS measurements were created for the targets. Here, all targets transmit AIS messages, which also include their width and length. All the targets are 6.63 meters long and 2.4 meters wide, the scenario lasts for 240 seconds, and the LiDAR measurements generate scans of the area at 1 Hz.

1) RESULTS

Figure 7 and Table 5 show the results. The targets enter and depart the surveillance area at different times, as can be seen by short spikes in the GOSPA values. These spikes correspond to missed detections when they arrive and false alarms when they leave, due to latency in the initialization and termination of tracks. Regardless, for most of the scenario the trackers are able to both track and estimate the extents of the targets quite successfully, with low localization error and high IOU. Use of AIS measurements both decreases the localization error and increases the IOU. This is shown throughout the whole scenario but is most evident before the 150 second mark. Here, occlusion effects result in low LiDAR measurement quality, which in turn makes it difficult to estimate the target states. AIS measurements, however, are not impacted by occlusion and allows the tracker to recuperate after the intermediate LiDAR scans. This effect becomes more evident because the AIS messages are transmitted at approximately the same time, resulting in noticeable spikes in the performance metrics also when averaging across all targets.

TABLE 5. Values for the performance metrics in Figure 7 and Figure 8. The values are averaged over the whole duration of the scenarios, and the best values for each metric are highlighted in bold.

	Simulated data		Experimental data	
	GP-PMBM	AIS-GP-PMBM	GP-PMBM	AIS-GP-PMBM
Total GOSPA	2.564	**1.420**	8.684	**4.789**
Localization	2.154	**1.091**	4.577	**3.693**
IOU	0.600	**0.765**	0.192	**0.263**

B. EXPERIMENTAL DATA

The experimental data used to test the AIS-GP-PMBM were collected in the Trondheim channel as part of the Autoferry project at NTNU, and was published in [45] as scenario 13. It is also discussed in the context of the GP-PMBM in [6]. The data were collected using a LiDAR mounted on the Milliampere ferry, which was stationary, with a range of approximately 60 meters. Furthermore, the scenario contains two targets, both 7 meters long and 3 meters wide motorboats. They travel across the length of the canal in opposing directions, passing each other approximately when closest to Milliampere. The targets did not transmit AIS messages, but GPS positions are available, which we

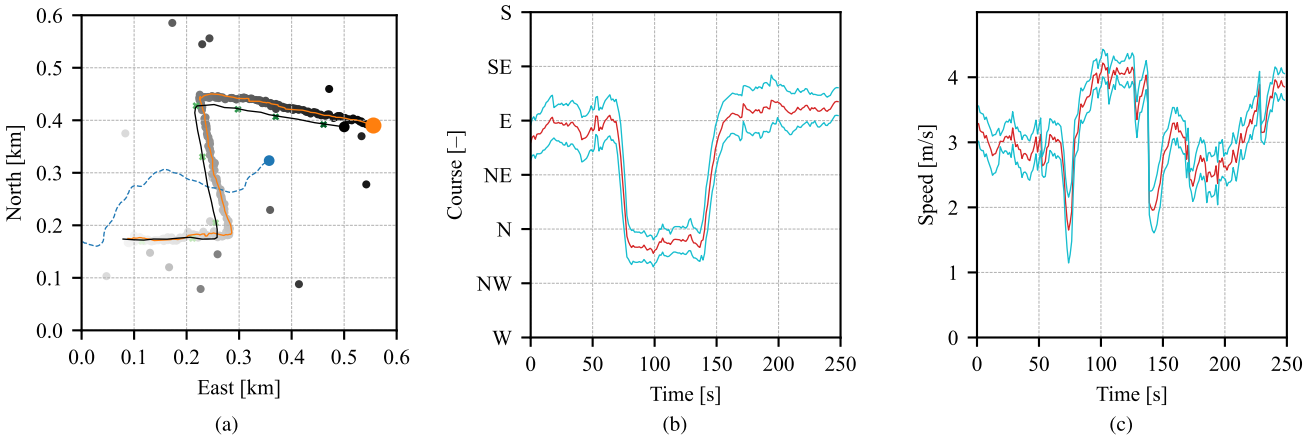

FIGURE 5. A scenario with a target conducting sharp and unpredictable maneuvers, showing how the tracker is able to successfully estimate the target state in a real-world setting. The ownship is shown as the dotted blue line in (a) and tries to move in a northeastern direction while upholding collision avoidance regulations. The target is shown as a solid orange line and tries to make maneuvers which hinder the Mariner in its objective. The radar measurements are shown as black dots which fade to grey as time passes, the AIS measurements are shown as green crosses which also fade as time passes, and the reported GPS position of the target is shown as a solid black line. (b) shows the evolution of the course estimates as a solid red line, together with one standard deviation in each direction as solid cyan lines. The speed estimates are shown in (c) in the same way, with the estimate as a red line and the standard deviations in cyan.

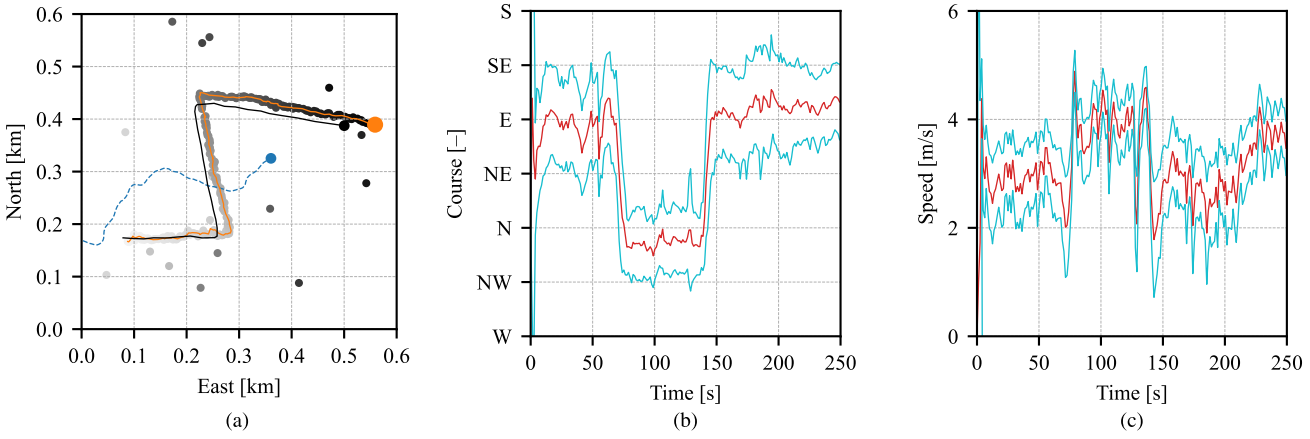

FIGURE 6. The same scenario as in Figure 5, but now an IPDA is used for tracking. an overview of the scenario is shown in (a), the estimated course is shown in (b), and the estimated speed is shown in (c). The tracker is able to follow the target, but the course and speed estimates are not as precise.

used to create AIS measurements in the same manner as previously.

1) RESULTS

The results can be seen in Figure 8 and Table 5. The overall performance is not as good as for the simulated data set. Because we are no longer dealing with simulated measurements that adhere to our modeling assumptions, this is to be expected. The ground truth also contains a bias which skews the results somewhat, but it is nevertheless useful for comparison purposes. Furthermore, the data set contains a lot of clutter, both from the ship wakes and other sources. The clutter model may struggle especially when encountering wake clutter. When evaluating the measurements in an association hypothesis, wake clutter will often be included and given a high weight. This leads to the extent estimate growing larger than it should, and the kinematic estimate being pulled towards the wake. Closely spaced targets which generate wake clutter can exacerbate performance degradation further by associating the wake clutter from one target with the other, and the tracker will figuratively try pulling the extent estimate apart. Some variation of this effect is seen in this data set, with the tracker struggling at the midpoint of the scenario when the targets are closest to each other.

Initially, both variations of the GP-PMBM are able to track the targets well, albeit with some false alarms for the pure LiDAR tracker. As the targets get closer to each other and the LiDAR, the performance degrades. The AIS-GP-PMBM is able to handle the situation better, helped by the AIS messages that both provide good kinematic information and the dimensions of the ship. In a situation where the LiDAR measurements cause the extent estimate to blow up, the AIS measurements help reduce its size. The pure LiDAR tracker,

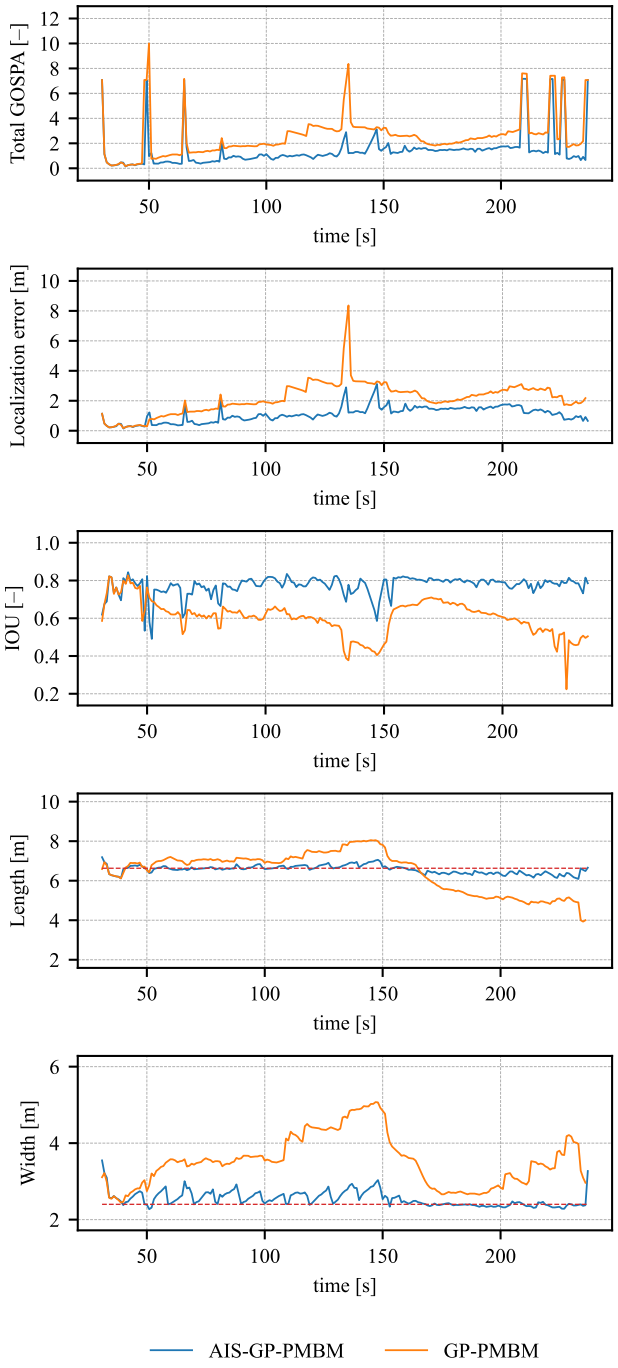

FIGURE 7. Comparison between the GP-PMBM and the AIS-GP-PMBM for the simulated data set. We use the GOSPA parameters $p = 2$, $c = 10$, and $\gamma = 5$. From top to bottom, the plots show the total GOSPA-T, the localization error, the IOU, the averaged estimated lengths, and the averaged estimated widths.

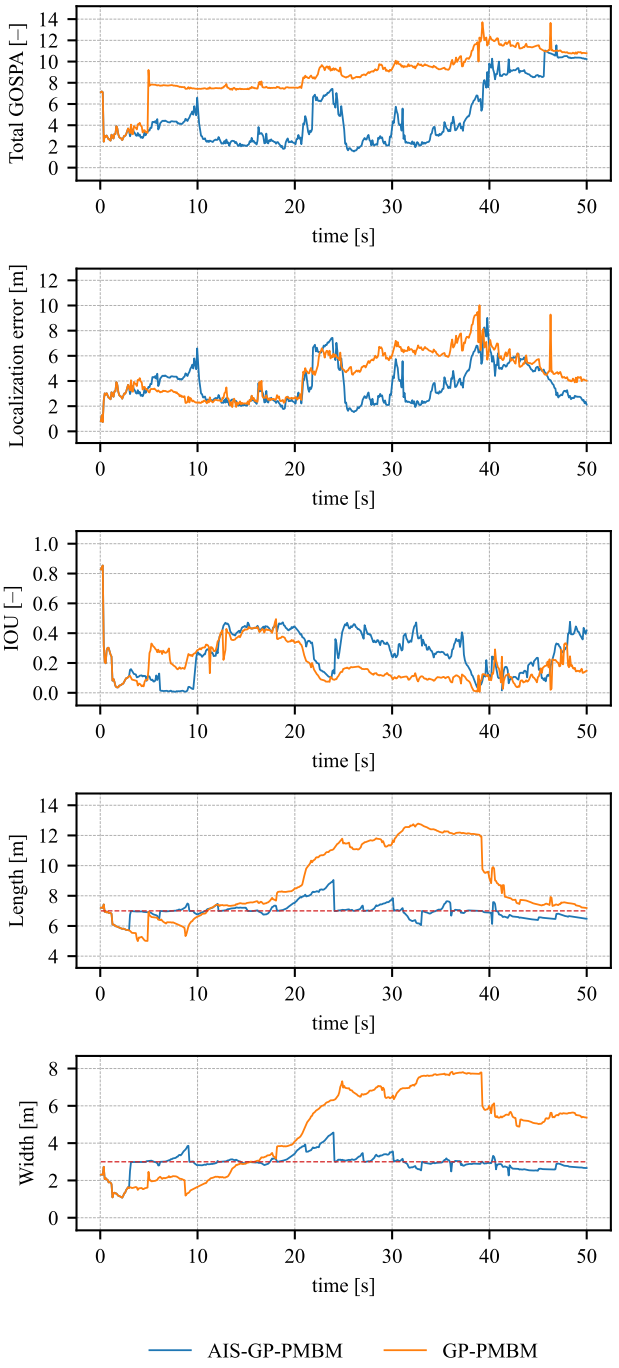

FIGURE 8. Comparison between the GP-PMBM and the AIS-GP-PMBM for the experimental data set. We use the GOSPA parameters $p = 2$, $c = 10$, and $\gamma = 5$. From top to bottom, the plots show the total GOSPA-T, the localization error, the IOU, the averaged estimated lengths, and the averaged estimated widths.

however, struggles to maintain a good extent estimate. This is seen clearly in the plots of the width and length, and in Figure 9. Furthermore, we see that the oversized extent of the non-AIS variant creates an offset in the position estimate, and that the direction of the estimate is flipped. At the displayed time step this is avoided when including AIS information, even though the heading is not directly updated with AIS information. Furthermore, false alarms are present for both trackers. For the pure LiDAR, tracker the false alarms are persistent throughout the whole scenario, whereas they arrive later in the scenario for the AIS-GP-PMBM. With a lot of clutter, and especially with wake clutter, this is difficult to mitigate without more advanced clutter models.

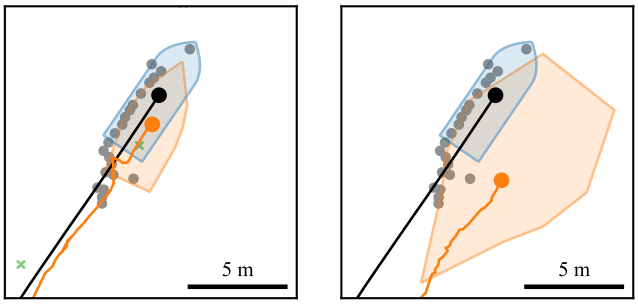

FIGURE 9. A snapshot of the extent of one of the targets 30 seconds into the scenario, at time step 283. The output from the AIS-GP-PMBM is shown in (a), and that of the GP-PMBM in (b). The estimated extent is shown in orange, and the ground truth in blue. Additional elements are explained in Figure 5. When not using AIS information, the extent estimate is both blown up and flipped orientation-wise.

VIII. CONCLUSION

We have presented a method for including target-provided information in PMBM trackers, with AIS messages as an example of such information. We do this for PMBM and its IMM-PMBM extension for point target tracking, and the GP-PMBM for extended objects. Through simulations and experiments we have shown that the AIS-PMBM and AIS-IMM-PMBM trackers perform better than their counterparts which do not use AIS measurements. Furthermore, we have compared the presented methods to other trackers which utilize AIS messages and shown that they perform well in comparison.

Because one of our use cases for the AIS-IMM-PMBM tracker is to provide target estimates for a collision avoidance system, we have also tested them in a closed-loop experiment. The results show that the AIS-IMM-PMBM tracker is able to provide good estimates and enables the collision avoidance method to respond to the target movements. The experiments also show the feasibility of using PMBM in applications which demand real-time performance.

Furthermore, we show how use of target-provided information in extended object tracking can mitigate some of the persistent problems when using only exteroceptive sensors. We use AIS, together with LiDAR, and use information regarding the ship dimensions to help estimate the extent. By updating the extent with the ship dimensions, we avoid that the extent changes its size when the LiDAR measurement quality is poor. We show that this can improve performance when a lot of clutter measurements are present, and that it helps the tracker recover from occlusion effects.

There are some potential lines of future research. Firstly, AIS messages can be utilized more extensively to improve target estimates. For example, they contain information about course, heading, and antenna placement, which can be useful in several ways. Furthermore, better wake clutter modeling can solve some of the problems encountered in Section VII-B. Several works present more general clutter models [46], [47], and also target-dependent clutter models for wake clutter mitigation [48], [49]. Such models could be utilized to improve the performance of the AIS-GP-PMBM in the presence of wake clutter.

ACKNOWLEDGMENT

The collision avoidance experiment was conducted in co-operation with Maritime Robotics, who provided personnel and infrastructure.

REFERENCES

[1] B.-n. Vo, M. Mallick, Y. Bar-shalom, S. Coraluppi, R. Osborne III, R. Mahler, and B.-T. Vo, "Multitarget tracking," in *Wiley Encyclopedia of Electrical and Electronics Engineering*. Hoboken, NJ, USA: Wiley, 2015, pp. 1–15.

[2] J. L. Williams, "Marginal multi-Bernoulli filters: RFS derivation of MHT, JIPDA, and association-based member," *IEEE Trans. Aerosp. Electron. Syst.*, vol. 51, no. 3, pp. 1664–1687, Jul. 2015.

[3] K. Granström, L. Svensson, Y. Xia, J. Williams, and A. F. Garcia-Fernandez, "Poisson multi-Bernoulli mixture trackers: Continuity through random finite sets of trajectories," in *Proc. 21st Int. Conf. Inf. Fusion*, Cambridge, U.K., Jul. 2018, pp. 973–981.

[4] E. F. Brekke and A. G. Hem, "A long simulation scenario for evaluation of multi-target tracking methods," in *Proc. 3rd Int. Conf. Electr., Comput., Commun. Mechatronics Eng. (ICECCME)*, Canary Islands, Spain, Jul. 2023, pp. 1–6.

[5] K. Granström, M. Fatemi, and L. Svensson, "Poisson multi-Bernoulli mixture conjugate prior for multiple extended target filtering," *IEEE Trans. Aerosp. Electron. Syst.*, vol. 56, no. 1, pp. 208–225, Feb. 2020.

[6] M. Baerveldt, M. E. López, and E. F. Brekke, "Extended target PMBM tracker with a Gaussian process target model on LiDAR data," in *Proc. 26th Int. Conf. Inf. Fusion (FUSION)*, Jun. 2023, pp. 1–8.

[7] Y. Xia, "Poisson multi-Bernoulli mixtures for multiple object tracking," Ph.D. dissertation, Dept. Elect. Eng., Chalmers Tekniska Hogskola, Sweden, 2022.

[8] H. A. P. Blom and Y. Bar-Shalom, "The interacting multiple model algorithm for systems with Markovian switching coefficients," *IEEE Trans. Autom. Control*, vol. AC-33, no. 8, pp. 780–783, Aug. 1988.

[9] G. Li, L. Kong, W. Yi, and X. Li, "Multiple model Poisson multi-Bernoulli mixture filter for maneuvering targets," *IEEE Sensors J.*, vol. 21, no. 3, pp. 3143–3154, Feb. 2021.

[10] International Telecommunication Union Radiocommunication Sector (ITU-R). (Feb. 2014) *Recommendation ITU-R M. 1371-5: Technical Characteristics for an Automatic Identification System Using Time Division Multiple Access in the VHF Maritime Mobile Frequency Band*. Accessed: Feb. 12, 2023. [Online]. Available: https://www.itu.int/rec/R-REC-M.1371-5-201402-I

[11] D. K. M. Kufoalor, E. Wilthil, I. B. Hagen, E. F. Brekke, and T. A. Johansen, "Autonomous COLREGs-compliant decision making using maritime radar tracking and model predictive control," in *Proc. 18th Eur. Control Conf. (ECC)*, Naples, Italy, Jun. 2019, pp. 2536–2542.

[12] B. Habtemariam, R. Tharmarasa, M. McDonald, and T. Kirubarajan, "Measurement level AIS/radar fusion," *Signal Process.*, vol. 106, pp. 348–357, Jan. 2015.

[13] D. Gaglione, P. Braca, G. Soldi, F. Meyer, F. Hlawatsch, and M. Z. Win, "Fusion of sensor measurements and target-provided information in multi-target tracking," *IEEE Trans. Signal Process.*, vol. 70, pp. 322–336, 2022.

[14] T. Miao, E. E. Amam, P. Slaets, and D. Pissoort, "Multi-target tracking and detection, fusing RADAR and AIS signals using Poisson multi-Bernoulli mixture tracking, in support of autonomous sailing," in *Proc. Int. Nav. Eng. Conf. Exhib. (INEC)*, Delft, The Netherlands, Oct. 2020, pp. 1–13.

[15] A. G. Hem and E. F. Brekke, "Variations of joint integrated data association with radar and target-provided measurements," *J. Adv. Inf. Fusion*, vol. 17, no. 2, pp. 97–115, Dec. 2022.

[16] Y. Bar-Shalom and E. Tse, "Tracking in a cluttered environment with probabilistic data association," *Automatica*, vol. 11, no. 5, pp. 451–460, Sep. 1975.

[17] T. Fortmann, Y. Bar-Shalom, and M. Scheffe, "Sonar tracking of multiple targets using joint probabilistic data association," *IEEE J. Ocean. Eng.*, vol. OE-8, no. 3, pp. 173–184, Jul. 1983.

[18] E. F. Wilthil, E. Brekke, and O. B. Asplin, "Track initiation for maritime radar tracking with and without prior information," in *Proc. 21st Int. Conf. Inf. Fusion (FUSION)*, Cambridge, U.K., Jul. 2018, pp. 1–8.

[19] D. Musicki, R. Evans, and S. Stankovic, "Integrated probabilistic data association (IPDA)," in *Proc. 31st IEEE Conf. Decis. Control*, Tucson, AZ, USA, Dec. 1992, pp. 3796–3798.
[20] D. Musicki and R. Evans, "Joint integrated probabilistic data association: JIPDA," *IEEE Trans. Aerosp. Electron. Syst.*, vol. 40, no. 3, pp. 1093–1099, Jul. 2004.
[21] D. Musicki and S. Suvorova, "Tracking in clutter using IMM-IPDA-based algorithms," *IEEE Trans. Aerosp. Electron. Syst.*, vol. 44, no. 1, pp. 111–126, Jan. 2008.
[22] D. Reid, "An algorithm for tracking multiple targets," *IEEE Trans. Autom. Control*, vol. AC-24, no. 6, pp. 843–854, Dec. 1979.
[23] K. Granström, M. Baum, and S. Reuter, "Extended object tracking: Introduction, overview and applications," *J. Adv. Inf. Fusion*, vol. 12, pp. 139–174, Dec. 2017.
[24] K. Gilholm, S. Godsill, S. Maskell, and D. Salmond, "Poisson models for extended target and group tracking," in *Proc. SPIE*, vol. 5913, San Diego, CA, USA, O. E. Drummond, Ed., Aug. 2005, pp. 230–241.
[25] J. W. Koch, "Bayesian approach to extended object and cluster tracking using random matrices," *IEEE Trans. Aerosp. Electron. Syst.*, vol. 44, no. 3, pp. 1042–1059, Jul. 2008.
[26] M. Baum and U. D. Hanebeck, "Shape tracking of extended objects and group targets with star-convex RHMs," in *Proc. 14th Int. Conf. Inf. Fusion*, Jul. 2011, pp. 1–8.
[27] N. Wahlström and E. Özkan, "Extended target tracking using Gaussian processes," *IEEE Trans. Signal Process.*, vol. 63, no. 16, pp. 4165–4178, Aug. 2015.
[28] R. Mahler, "PHD filters for nonstandard targets, I: Extended targets," in *Proc. 12th Int. Conf. Inf. Fusion*, Jul. 2009, pp. 915–921.
[29] K. Granstrom and U. Orguner, "A phd filter for tracking multiple extended targets using random matrices," *IEEE Trans. Signal Process.*, vol. 60, no. 11, pp. 5657–5671, Nov. 2012.
[30] K. Granström and U. Orguner, "Estimation and maintenance of measurement rates for multiple extended target tracking," in *Proc. 15th Int. Conf. Inf. Fusion*, Jul. 2012, pp. 2170–2176.
[31] C. Lundquist, K. Granström, and U. Orguner, "An extended target CPHD filter and a gamma Gaussian inverse Wishart implementation," *IEEE J. Sel. Topics Signal Process.*, vol. 7, no. 3, pp. 472–483, Jun. 2013.
[32] E. Liland, "AIS aided multi hypothesis tracker," Master's thesis, NTNU, Trondheim, Norway, 2017.
[33] E. F. Brekke, A. G. Hem, and L. N. Tokle, "Multitarget tracking with multiple models and visibility: Derivation and verification on maritime radar data," *IEEE J. Ocean. Eng.*, vol. 46, no. 4, pp. 1272–1287, Oct. 2021.
[34] Y. Bar-Shalom, X. R. Li, and T. Kirubarajan, *Estimation With Application to Tracking and Navigation*. Hoboken, NJ, USA: Wiley, 2001.
[35] A. G. Hem and E. F. Brekke, "Compensating radar rotation in target tracking," in *Proc. Sensor Data Fusion: Trends, Solutions, Appl. (SDF)*, Oct. 2022, pp. 1–6.
[36] Á. F. García-Fernández, J. L. Williams, K. Granström, and L. Svensson, "Poisson multi-Bernoulli mixture filter: Direct derivation and implementation," *IEEE Trans. Aerosp. Electron. Syst.*, vol. 54, no. 4, pp. 1883–1901, Aug. 2018.
[37] K. G. Murty, "Letter to the editor—An algorithm for ranking all the assignments in order of increasing cost," *Operations Res.*, vol. 16, no. 3, pp. 682–687, Jun. 1968.
[38] K. Granström, L. Svensson, S. Reuter, Y. Xia, and M. Fatemi, "Likelihood-based data association for extended object tracking using sampling methods," *IEEE Trans. Intell. Vehicles*, vol. 3, no. 1, pp. 30–45, Mar. 2018.
[39] M. Longbin, S. Xiaoquan, Z. Yiyu, S. Zhong Kang, and Y. Bar-Shalom, "Unbiased converted measurements for tracking," *IEEE Trans. Aerosp. Electron. Syst.*, vol. 34, no. 3, pp. 1023–1027, Jul. 1998.
[40] Á. F. García-Fernández, A. S. Rahmathullah, and L. Svensson, "A metric on the space of finite sets of trajectories for evaluation of multi-target tracking algorithms," *IEEE Trans. Signal Process.*, vol. 68, pp. 3917–3928, 2020.
[41] A. F. Garcia-Fernandez. *MTT*. Accessed: Oct. 8, 2023. [Online]. Available: https://github.com/Agarciafernandez/MTT
[42] A. G. Hem, E. F. Brekke, G. D. K. M. Kufoalor, and I. H. Kingman, "Autonomous marine collision avoidance with sensor fusion of AIS and radar," in *Proc. 15th IFAC Conf. Control Appl. Marine Syst., Robot. Vehicles (CAMS)*, 2024, pp. 1–6.
[43] D. K. M. Kufoalor, T. A. Johansen, E. F. Brekke, A. Hepsø, and K. Trnka, "Autonomous maritime collision avoidance: Field verification of autonomous surface vehicle behavior in challenging scenarios," *J. Field Robot.*, vol. 37, no. 3, pp. 387–403, Nov. 2019.
[44] B. H. Eriksen, E. F. Wilthil, A. L. Flaten, E. F. Brekke, and M. Breivik, "Radar-based maritime collision avoidance using dynamic window," in *Proc. IEEE Aerosp. Conf.*, Big Sky, MT, USA, 2018, pp. 1–9.
[45] Ø. K. Helgesen, K. Vasstein, E. F. Brekke, and A. Stahl, "Heterogeneous multi-sensor tracking for an autonomous surface vehicle in a littoral environment," *Ocean Eng.*, vol. 252, May 2022, Art. no. 111168.
[46] B.-T. Vo, B.-N. Vo, and A. Cantoni, "Bayesian filtering with random finite set observations," *IEEE Trans. Signal Process.*, vol. 56, no. 4, pp. 1313–1326, Apr. 2008.
[47] Á. F. García-Fernández, Y. Xia, and L. Svensson, "Poisson multi-Bernoulli mixture filter with general target-generated measurements and arbitrary clutter," *IEEE Trans. Signal Process.*, vol. 71, pp. 1895–1906, 2023.
[48] E. Brekke, O. Hallingstad, and J. Glattetre, "Improved target tracking in the presence of wakes," *IEEE Trans. Aerosp. Electron. Syst.*, vol. 48, no. 2, pp. 1005–1017, Apr. 2012.
[49] A. G. Hem, H.-G. Alvheim, and E. F. Brekke, "WakeIPDA: Target tracking with existence modeling in the presence of wakes," in *Proc. 26th Int. Conf. Inf. Fusion (FUSION)*, Jun. 2023, pp. 1–7.

AUDUN G. HEM received the M.Sc. degree in engineering cybernetics from Norwegian University of Science and Technology (NTNU), in 2021, where he is currently pursuing the Ph.D. degree with the Department of Engineering Cybernetics. He specializes in data fusion and target tracking for autonomous surface vehicles. He is also involved in the Autosit Project.

MARTIN BAERVELDT received the M.Sc. degree in complex adaptive systems from Chalmers University of Technology, Gothenburg, Sweden, in 2019. He is currently pursuing the Ph.D. degree with the Department of Engineering Cybernetics, Norwegian University of Science and Technology (NTNU). He is a part of European training and research network on autonomous barges for smart inland shipping (AUTOBarge). His research interests include automated situational awareness with a view to autonomous surface vessels, with a particular focus on extended object tracking.

EDMUND F. BREKKE (Senior Member, IEEE) received the M.Sc. degree in industrial mathematics and the Ph.D. degree in engineering cybernetics from Norwegian University of Science and Technology (NTNU), Trondheim, Norway, in 2005 and 2010, respectively. From 2010 to 2014, he was with the Acoustic Research Laboratory (ARL), NUS, Singapore, as a Postdoctoral Research Fellow. In 2014, he rejoined NTNU and the Department of Engineering Cybernetics and is currently a Professor of sensor fusion. This position was funded as a gift professorship by DNV, from 2014 to 2019. He was the Project Manager of the Autosea Project, developing methods for sensor fusion and collision avoidance for autonomous surface vehicles. He is also a Key Scientist for the Autoferry Project, which is focused on autonomous pedestrian ferries, the Work Package Manager of the Centre for Research-based Innovation SFI Autoship, and the Project Manager of the Autosit and Autosight projects, which are focused on automated situational awareness for autonomous surface vehicles. His research interests include sensor fusion and situational awareness, with a particular focus on multi-target tracking. He is an Associate Editor of the IEEE JOURNAL OF OCEANIC ENGINEERING.